Application of numerical treatment of wake by Simplified Methods.

Effects of simple generic configuration on near to far field wake by using 3D Vortex Filament Method.

C-Wake Report UPS-PR 2.2.3-2

D. Margerit, P. Brancher and A. Giovannini

IMFT, Allée du professeur Camille Soula, 31400 Toulouse, France

C-Wake Project GRD1-1999-10332

Application of numerical treatment of wake by Simplified Methods.

Effects of simple generic configuration on near to far field wake by using 3D Vortex Filament Method.

C-Wake Report UPS PR 2.2.3-2

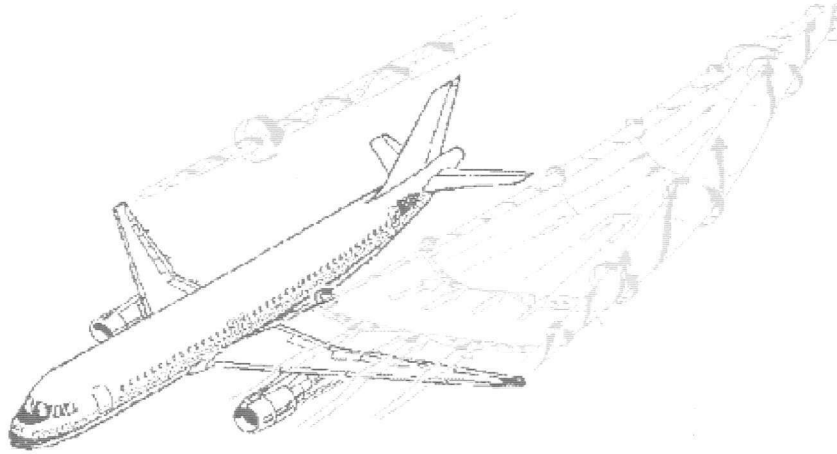

C-Wake Project GRD1-1999-10332

Prepared by: **D. Margerit, P. Brancher and A. Giovannini(UPS)**

Document control data

Deliverable No. :	**PR 2.2.3-2**	Approved by D. Darracq (Cerfacs)
Work Package:	**WP 2.2.3**	Reviewed by:
Version:	**1**	F. Laporte (Cerfacs)
Date of issue:	**28-02-2002(month 25)**	

Summary

As part of Task 2.2.3 of the C-Wake Project a computational code EZ-vortex is developed for the motion of slender vortex filaments. We chose to implement a *Slender* Vortex Filament code rather than a standard Vortex Filament one as it gives *fast* computation which is a requirement of our task. This code is useful to have fast computation of the far field wake. The integro-differential equations governing the motion of the vortex centerlines are either the Callegari and Ting equations, which are the leading order solution of a matched asymptotic analyses, or equivalent forms of these equations. They include large axial velocity and non-similar profiles in the vortical cores. The fluid may be viscous or inviscid. This code is validated both against known solutions of these equations and results from linear stability analysis. The linear and non-linear stages of perturbed two-vortex and four-vortex wakes have been computed and tested.

The analysis of the NLR experimental results in LST and LLF wind tunnels has been completed to obtain the physical parameters needed as an input of our code. As there are no long wavelength 3D effects in these near- and mid- field experimental results, the physical parameters of the last cross sections were extracted by our analysis from the data files and are used as an input of our code by giving the initial conditions for the temporal computation of the far field. We have done the computations for configurations 1, 2, 3, and 6 of NLR experimental data: this is our parametric study of the NLR results.

It appears that our code needs to be coupled with near- and mid- field results to do a parametric study with the wing parameters as an input. It is the only fast computation code of the far field. It gives accurate results up to the trailing pair reconnection. It is a useful tool to compute this part of the wake and it may be used to compare far field experimental data from catapult, tower tank or flight measurements in real atmosphere. As a perspective a fast engineering code could be developed from this code by adding 3D models of reconnection so that to continue the computation through the trailing pair reconnection.

Contents

I. INTRODUCTION

The potential hazard related to the two-vortex aircraft wake induces separation distances between aircrafts and associated delay at landing and take-off, which contributes to the congestion of airports [1–3]. Present ICAO separation rules in forces are conservative to minimize the risk of a possible wake encounter. Separation distances -based on aircraft weight- are empirical.

It was therefore considered indispensable to address, within the 5th Framework Program of the EC, the Wake Vortex Characterization and Control. The C-Wake project addresses the three following aspects: i) the physical aspects of a wake through wake characterization; ii) it produces application guidelines for the European aircraft industry on how to control the wake vortex size and intensity; iii) it synthesizes findings in order to arrive at a validated method of predicting a Large Transport Aircraft-Type's wake characteristics with sufficient accuracy.

As to better understand the interest of our work in subtask 2.2.3 of this project, it may be interesting to sketch a quick overview of the C-Wake organization. The C-Wake project consists of experimental work (Work Package 1 [WP1]), numerical and theoretical work (WP2) and a synthesis task (WP3) as can be seen in Fig. 1. WP2 consists of numerical computation of the near field (Task 2.1), far field extrapolation of near field result and prediction (Task 2.2) and theoretical study of unsteady effects (Task 2.3). Task 2.2 studies the effect of modifications to generic wing on far field wake (Subtask 2.2.1), the effect of design modifications to Airbus-type aircraft wing on wake (Subtask 2.2.2) and the configuration assessment by simplified methods (Subtask 2.2.3).

We are the only one in subtask 2.2.3 who use a fully 3D method. Our goal is to study the effect of a simple geometric configuration on near to far field wake by using 3D vortex filament methods. As it was defined in the C-Wake initial Project [4], our work is in four steps: i) adaptation of a vortex filament method, ii) acceleration of the method, iii) validation and iv) parametric study. It lasts from the middle of March 2000 to the end of February 2002.

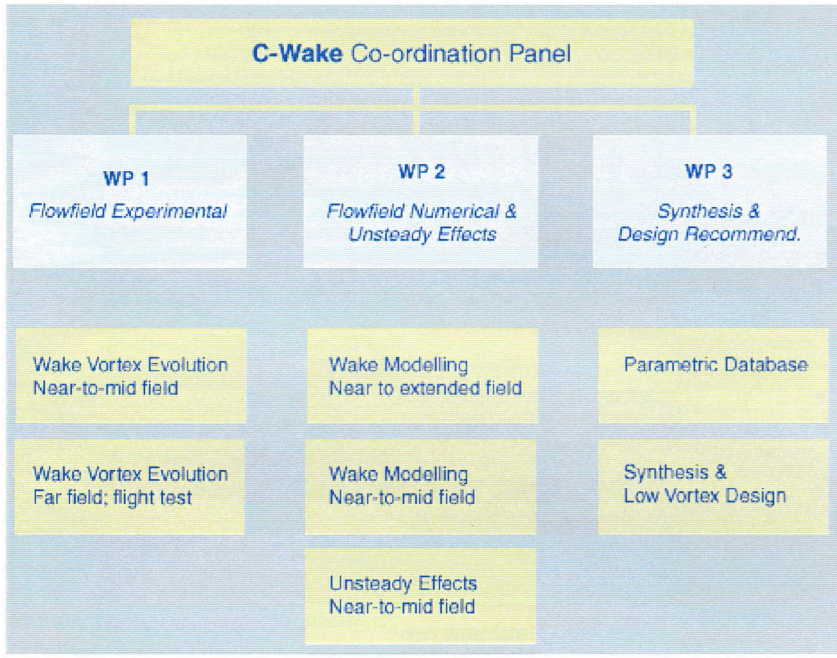

FIG. 1. C-Wake organisation

Vortex methods [5–8] are numerical methods of great interest to study *vortical flows*. The discretization is of the vorticity field, rather than the velocity field, and is Lagrangian in nature. It consists of a collection of particles (Vortex Particle methods [VP]) or filaments (Vortex Filament methods [VF]) which carry concentrations of vorticity. The velocity field is recovered from the discretized vorticity field via the Biot-Savart law and a *numerical smoothing parameter* is introduced to desingularize the Biot-Savart line-integral kernel. The vorticity field is then evolved in time according to this velocity field.

We have implemented [9] a *slender* vortex filament (SVF) code based on asymptotic equations of motion [10–12] derived by Callegari and Ting from the Navier-Stokes equations in the slenderness limit. For a closed vortex let us briefly introduce this equation which is the heart of our work. A *slender vortex ring* of circulation

Γ is a field of vorticity which is non-zero only in the neighbourhood of a three-dimensional curve $\mathcal{C}$, called the *centerline*. This curve is described parametrically by a function $\mathbf{X} = \mathbf{X}(s,t)$ which denotes a point on the curve as a function of the parameter s, with $s \in [-\pi, \pi[$, and the time t. For each point on the curve $\mathcal{C}$, the Frenet frame $(\mathbf{t}, \mathbf{n}, \mathbf{b})$ is defined with respectively the tangent, normal and binormal vectors. The thickness δ of the ring is of order l and the other length scales, for example the local *curvature* K or the length S of $\mathcal{C}$ are of the same order L. Since the vortex is slender, a small parameter $\varepsilon \ll 1$ is defined as the ratio l/L. The velocity field is non-dimensionalized using Γ/L, all lengths using L, and the time using L^2/Γ. The equation of motion of a *non-circular* slender vortex ring has been derived by CT from the Navier-Stokes equations using a matched asymptotic expansion in ε. At leading order the following equation was obtained

$$\partial\mathbf{X}/\partial t - [\partial\mathbf{X}/\partial t \cdot \mathbf{t}]\,\mathbf{t}(s,t) = \mathbf{Q}(s,t) + K(s,t)\,[-\ln\varepsilon + \ln S(t) - 1 + C_v(t) + C_w(t)]\,\mathbf{b}(s,t)/4\pi, \tag{1}$$

where $\mathbf{Q}(s,t)$ is an integral given by $\mathbf{Q}(s,t) = \mathbf{A}(s,t) - [\mathbf{A}(s,t)\cdot\mathbf{t}(s,t)]\,\mathbf{t}(s,t)$ with

$$\mathbf{A}(s,t) = \frac{1}{4\pi}\int_{-\pi}^{\pi} \sigma(s+s',t)\left[\frac{\mathbf{t}(s+s',t)\times(\mathbf{X}(s,t)-\mathbf{X}(s+s',t))}{|\mathbf{X}(s,t)-\mathbf{X}(s+s',t)|^3} - \frac{K(s,t)\mathbf{b}(s,t)}{2\,|\lambda(s,s',t)|}\right] ds'.$$

Here $\sigma(s,t) = |\partial\mathbf{X}/\partial s|$ and $\lambda(s,s',t) = \int_s^{s+s'} \sigma(s^*,t)ds^*$. In equation (1) $C_v(t)$ and $C_w(t)$ are known functions (see [10]) depending on the inner structure of the vortex at leading order in ε.

Using the Callegari and Ting's equation Klein and Knio [11] have shown that it is not correct to compute a vortical flows composed of several thin vortex filaments by a standard vortex filament (VF) method with only one *numerical filament* per section of the thin vortex filaments (the so called thin-tube model): more than one numerical filament per section is needed to insure the convergence of the numerical scheme. However, as it would save computation time to have only one numerical filament per section, Klein and Knio [11] proposed a cure: they have shown how to adjust the numerical desingularization parameter (the so called thin-tube thickness) to real thickness of the slender vortex filaments so that the method gives correct results. As the corrected thin-tube model is still stiff to be solved numerically Knio and Klein [12] removed this stiffness in the *improved thin tube models* that they proposed.

We have adapted this numerical scheme for open vortex filaments which are periodic with a characteristic wavelength and we have implemented it in a code named EZ-Vortex. The fluid may be viscous or inviscid; the relative velocity field (*i.e.* velocity field minus filament velocity) is axisymmetric and may be similar (*i.e.* Gaussian) or not (it can be a Rankine vortex or any axisymmetric vorticity profile). The evolution of the core structure (diffusion and stretching) is taken into account in the asymptotic equation and so in the implemented code.

Among the 3D vortex methods we have chosen to implement a Slender Vortex Filament method because it is adapted to solve vortical flows composed of several thin vortex filaments as is a wake vortex in the far field. A brief overview of the different vortex methods and of their characteristics are given in Appendix A. A complete description of the slender vortex governing equations is given in Appendix B. The implemented code EZ-vortex provides a useful and *fast* tool for the simulation of aircraft wakes in the far field. As we only consider computations in the far field we direct the readers interested by three-dimensional vortex filament method in the near field to the paper of Ehret *et al.* [13]. The thickness of the vortex core found in the wind tunnel experiments [14] confirms the slenderness assumption: the vortex core thickness over the distance of the trailing vortices is found to be of a few percents. We have implemented [9] a slender vortex filament method because the cost of computation is smaller with this method than with Vortex Blob Methods or Vortex Filament Methods [15]. This method is fast as it is based on the equation of motion obtained from an asymptotic expansion of the Navier-Stokes equations in terms of the small thickness of these vortices. This method takes advantages of a great theoretical work [10–12] in which lots of analytical calculus were carried out so as to take advantage of the slenderness in order to obtain a simplification of the Navier-Stokes equations and to avoid the stiffness of these equations which is inherent in this limit. A fully resolved 3D computation with a standard Vortex Filament Method would have the same computational cost as a DNS of the Navier-Stokes equations. It would be outside of the simplified and fast computation requirement of task 2.2.3. In literature fully resolved computations with 3D vortex Methods of the same cost as LES are under consideration by developing sub-grid models adapted for vortex methods [16].

Section II of this report explain the implementation of the EZ-Vortex code. We first implemented the Callegari and Ting equation of motion for closed and open filament with Gaussian core. Then we have extended the slender-vortex-filament code EZ-Vortex to non-Gaussian vorticity in the vortex core and we have also implemented the M1-method of Knio and Klein [12] because the line integral of this method is simple to compute and because the time stepping can be explicit and allows to use an Adams-Bashforth time stepping which is second order. Spatial derivatives can also been computed spectrally for closed and open filaments. In this code

we use a drawing of the filament at run time with the OpenGL library on a SGI workstation. The philosophy of EZ-Vortex code is to keep programs as simple as possible and to provide documentation both by way of a text [17] and of comments within the code itself. Appendix C gives the features of this code: it is the documentation of this code [17]. We chose to have physical parameters in dimensional form as an input of EZ-Vortex. In this way EZ-Vortex can perform both dimensional or non-dimensional runs.

In section III we give the validation of this this code for open vortex filaments against the linear stability analysis of a two-vortex and four-vortex aircraft wake configurations. The amplification rate of unstable modes of the Crow instability for two trailing vortices have been checked and also the period of oscillations of stable modes. For the four-vortex wake the base flow is the stationary four vortices. The rate of growth and the wavelength of the instability that we obtained compare favorably with the ones of Fabre and Jacquin [18,19] who obtained their results from a linear stability analysis. Rennich and Lele [20] have shown that the destruction of aircraft wake vortices can be accelerated by adding two flap-vortices between the trailing-edge vortices. Their results were obtained both from a Navier-Stokes spectral code and from a *simple* vortex filament code. Our code allows us to improve the previous results of Rennich and Lele [20]. Appendix D gives the validation for closed vortex filaments and for other linear stability results. We analyze the influence of all the numerical parameters to be sure to have converged results. In EZ-Vortex both viscosity and vortex stretching are taken into account. The vortex stretching is not local as it is in the slenderness limit [21,22] and no axial core variations are taken into account because it takes place on a very fast time [22]. For other Kelvin-wave phenomena the reader is directed to the recent overview of M. Rossi [23]. The description of the slender vortex method and the validation of EZ-vortex with stability results have been written in a paper [9] which has been submitted.

In section IV we give a brief overview of LST and LLF wind tunnel results given by NLR. These experimental results are for a generic model: the SWIM model geometry, and consist in 6 model configurations. The LST results are closer to the wing than the LLF one. We have to use these data as initial conditions of our numerical computations. In September 2001 we got from NLR a set of 6 CD-Roms [24] with LST results and the associated report [14]. There are no LLF results in these CDs nor rake data with LST. Contrary to rake data, some PIV results with LST are unable to give the velocity field inside the vortices. Moreover rake data also give the axial velocity component. In the beginning of September 2001 we got from NLR 1 CD-Rom [25] with all results: LST (PIV and Rake) and LLF; and the associated report [26]. In these new data files the axial vorticity component has already been computed. For most files the velocity field which was in several data files in the previous CDs have been interpolated on a grid for the whole wake domain (behind the left and right hand wings). These files make the experimental results far easier to handle. A correction was done to the velocity field in an last report [27]. In order to generate the initial conditions of the EZ-vortex code from these experimental data we need to have a physical analysis of the flow, i.e. to have the physical parameters: *number of vortices, their circulation, position and thickness.* Unfortunately most of these parameters (individual circulation and thickness) are not given in the NLR analysis report [26]. As we need it we have completed the analysis of NLR by computing these physical parameters for the different experimental data files. An overview of this analysis is given in this section IV. As can be seen from data files of NLR, there is no long wavelength 3D effect in these experiments. There is first a merging of for filaments with either a 2D merging or a short wavelenght instability merging and then a 2D motion of the two trailing vortices. As our code captures 3D curvature long wavelength effect, it is a useful tools to extrapolate these experimental mid field to the far field by using the last cross section velocity field. The analysis of the different last cross sections is carried out and we give in this section IV the values of the physical parameters needed for the parametric study of next section.

In section V we carried out the computations of the different cases obtained in section IV. We then conclude in section VI and give perspectives of this work and of the EZ-vortex code which has been proved to be of great use for far field computations.

As was planned in the C-Wake initial Project [4], our work is in four steps: i) adaptation of a vortex filament method,ii) acceleration of the method, iii) validation and iv) parametric study with the use of NLR wind tunnel experimental results on a generic model: the SWIM model. Sections I and II are devoted to the two first steps i) and ii): here the acceleration of the method was obtained by the choice of the implementation of a Slender Vortex Method. In the choice of a standard Vortex Method the acceleration phase would have corresponded to the implementation of a fast Poisson solver or of other tricks to accelerate the computation. Sections III is devoted to the third steps iii) and sections IV and V to the parametric study step iv).

II. IMPLEMENTATION OF EZ-VORTEX: A SLENDER VORTEX FILAMENT CODE

The EZ-vortex code [17] is the numerical implementation of the Callegari and Ting equation (see Eqs. (B1), (B2), (B3), and (B5) in Appendix B) for closed filaments and of the associated versions for open filaments (see Eq. (B12) in Appendix B). The philosophy of the code is to keep programs as simple as possible and to provide

documentation both by way of a text [17] and comments within the code itself. It will be available through the world-wide web and is adapted from the code EZ-Scroll developed by Dwight Barkley for simulating scroll waves in excitable media [28,29]. This package uses OpenGL for 3D rendering or the Mesa library (public domain implementation of most OpenGL routines). It should be possible to run on virtually any machine supporting X. Setting macros of the C-preprocessor (defined in the main header file) to 0 or 1 allows to have a conditional compilation of the code and to have a unique source-code with different equations of motion and with different spatial and temporal numerical discretizations.

The *physical* parameters in the simulation are the initial stretched core radius δ_0, the initial axial flux m_0, the circulation Γ, the aspect ratio parameter $\varepsilon = \delta/L$, and the stretched viscosity $\nu = \nu/\varepsilon^2$ of the fluid. The *numerical* parameters for the simulation are the number np of spatial points (nodes) on each filament, the time step dt, the number nsteps of time steps and nb the number of periodic boxes for open filaments (see Fig.2).

A. Spatial discretization

The curve $\mathbf{X}$ is discretized by putting np points on the centerline, *i.e.* by an uniform discretization of the interval $s \in [-\pi, \pi[$.

1. Derivatives

First-derivative $\sigma\mathbf{t} = \partial\mathbf{X}/\partial s$ and second-derivative $K\mathbf{b} = \partial\mathbf{X}/\partial s \times \partial^2\mathbf{X}/\partial s^2/|\partial\mathbf{X}/\partial s|^3$ are approximated by second order centered differences or spectrally computed via a Fast Fourier Transform (FFT). For periodic open filaments of period $\Lambda(t)$ in the $\mathbf{e}_x$ direction $[\mathbf{X}(s+2\pi,t) = \mathbf{X}(s,t) + \Lambda(t)\mathbf{e}_x]$ the following periodic function $\tilde{\mathbf{X}}(s,t) = \mathbf{X}(s,t) - \Lambda(t)s/(2\pi)\mathbf{e}_x$ is defined. As it satisfies $\tilde{\mathbf{X}}(s+2\pi,t) = \tilde{\mathbf{X}}(s,t)$ its derivatives can be spectrally computed via a FFT as for the closed filament. The first-derivative is then given by $\partial\mathbf{X}/\partial s = \partial\tilde{\mathbf{X}}/\partial s + \Lambda(t)/(2\pi)\mathbf{e}_x$ and the second-derivative by $\partial^2\mathbf{X}/\partial s^2 = \partial^2\tilde{\mathbf{X}}/\partial s^2$.

2. Integrals

The trapezoidal rule is used to compute any integral part of the equation of motion. In case of a periodic open filament we take advantage of the periodicity and advance in time only a part of the filament (see Fig.2) corresponding to a period $\Lambda(t)$ (or an integer number of periods). The self-induction at point $\mathbf{X}(s,t)$ on this part of the filament is found by adding two contributions (see Fig.2). The first one is the self-induction of a bit of filament in a box of length $\Lambda(t)$ centered on $\mathbf{X}(s,t)$. The second is the induction of the remaining part of the open filament in nb boxes of length $\Lambda(t)$ from both sides of the central box. The self-induction part is obtained with one of the equations (B1), (B2), (B3) or (B5) for a closed filament and the remaining part is obtained with the mutual induction velocity formula (B11) as if it were coming from other filaments.

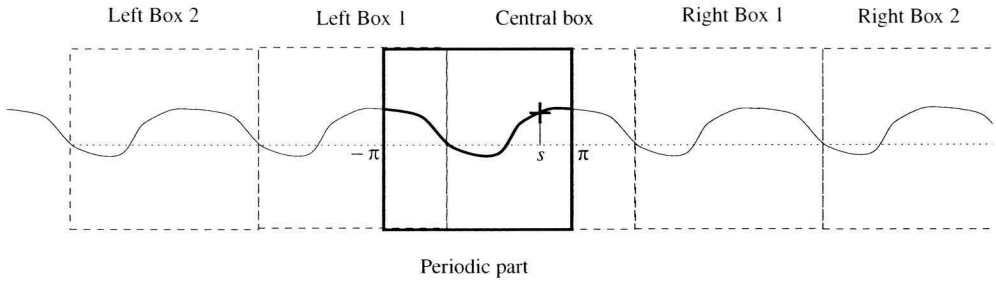

FIG. 2. Periodic part of the filament, central box around $\mathbf{X}(s,t)$ and left and right side boxes.

The spatial discretization can be checked at initial time by testing the convergence of the Biot-Savart velocity computation with the number of points and with the number of periodic boxes for open filaments.

B. Temporal discretization

The time stepping of the equation of motion is either an explicit forward Euler first-order scheme, an implicit backward Euler first-order scheme with an iterative sequel that converges to the solution of the non-linear algebraic system, or an Adams-Bashforth second-order explicit scheme. Explicit schemes can also be done *on place*, *i.e.* without a temporary variable for the coordinate positions for the nodes of the filament.

Explicit schemes for equations with a local $K\mathbf{b}$ term [Callegari and Ting (B1) or LIA (B2)] are always unstable [30] and are conditionally stable for the simple de-singularized method (B3) or for the M1 de-singularized method (B5) of Knio and Klein. An Adams-Bashforth second-order explicit scheme can be used with these later methods. Moreover (B3) and (B5) need not to compute the local $K\mathbf{b}$ term and are also easier to implement because their non-local integral term is a simple expression whereas in the Callegari and Ting equation (B1) the integrand of the integral term $\mathbf{A}$ is a subtraction of two terms and needs the computation of the $K\mathbf{b}$ term and of the integral distance function $\lambda(s, s', t)$. The M1 de-singularized method of Knio and Klein (B5) is more advantageous than the simple de-singularized method (B3) because contrary to this later method it is not stiff in the small thickness parameter ε : as can be seen from direct numerical computation the simple de-singularized method (B3) needs much more number of points to converge than the M1 de-singularized method of Knio and Klein. It is interesting to have implemented all these different methods in order to compare their different advantages from direct numerical computation and to avoid any implementing mistake by checking their convergence to the same result. The convergence of every simulation is assessed by increasing the number of points and by decreasing the time step.

C. Closed and open filament storage

In this subsection we explain the choices that we did to implement the numerical schemes. It is of interest for anyone who would like to do such an implementation or go through the lines of the EZ-vortex code. Cartesian coordinates (x, y, z) of nodes i on the filament j are successively stored in a pointer u and are managed by three macros Ux(i,j), Uy(i,j), Uz(i,j), where Ux(i,j) is the coordinate x of the node i on the filament j. The same kind of pointer (u_s, u_ss, ...) and macros are used for the first and second derivatives, for σ and for the velocity components. The index i ranges from 0 to np+1 and the index j from 0 to nf−1, where np and nf are respectively the number of nodes and of filaments. Points 0 and np+1 are added-fictitious points which may be of use.

For a closed filament the point of index np is at the same location as the point of index 1, whereas for an open filament the point of index np is the translated point [with period $\Lambda(t)$] of the point of index 1. In the spectral computation of the derivatives the FFT routine uses the points from $i = 1$ to $i = \mathsf{np} - 1$ and the index $\mathsf{np} - 1$ is 256. For closed filaments we find the induced velocity on nodes $i = 1$ to $i = \mathsf{np} - 1$ (respectively $i = \mathsf{np}$ for open filament) and then move all these points.

For open filaments the self-induced velocity at any point $\mathbf{X}(s, t)$ of index i is found as displayed in Fig.2: temporary pointers (ux_tmp, uy_tmp, uz_tmp) are introduced to store part of the filament in the *central box* around this point i which is stored at the central index $(\mathsf{np} + 1)/2$ of these pointers (the number of points np is an odd number). The same temporary pointers are also used for closed filaments. With these temporary pointers the same procedure is then used to compute the velocity whatever point is under consideration. The procedure to fill these pointers is different whether the filament is closed or open because indices have to be managed differently. For open filaments the induced velocity of the nb copies on the left and right boxes is added to the self-induced velocity of the central part.

D. Description of EZ-Vortex

The principal features of the code EZ-Vortex, the way to run it and to use it is given in the EZ-Vortex documentation [17]. You can find this documentation in Appendix C.

III. VALIDATION OF EZ-VORTEX

Appendix D gives the validation for closed vortex filaments and for other linear stability results. In this section the EZ-vortex code is validated against linear stability results of a two and four aircraft wake. We also analyse the influence of all the numerical parameters to be sure to have converged results.

A. Study of a two-vortex aircraft wake

In this subsection the EZ-vortex code is used to study a two-vortex aircraft wake which consists in a pair of contra-rotating vortex filaments. It gives a validation of the code. All following simulations use the M1 de-singularized method of Knio and Klein with the explicit Adams-Bashforth scheme and with $\Gamma = \pm 1$. There is no axial flow ($m_0 = 0$) and the fluid is inviscid ($\nu = 0$). Here, the vortex core is a *similar vortex* profile. The initial reduced thickness is $\delta_0 = 1$ and so the small parameter ε is the initial thickness δ_0. The velocity of the contra-rotating vortex filament pair of circulation $\pm\Gamma$ is $V = \Gamma/2\pi L$, where L is the distance between the vortices. We checked that the code reproduces this velocity (data not shown). The stability diagrams can be deduced from the study of Crow [31] and are recalled in figure 3. Here, we chose to display the wavelength instead of the wavenumber and to plot the diagrams as a function of the initial thickness ε rather than the ad-hoc cut-off length of Crow [31]. These diagrams are in dimensionless form ($L = 1$ and $\Gamma = \pm 1$.)

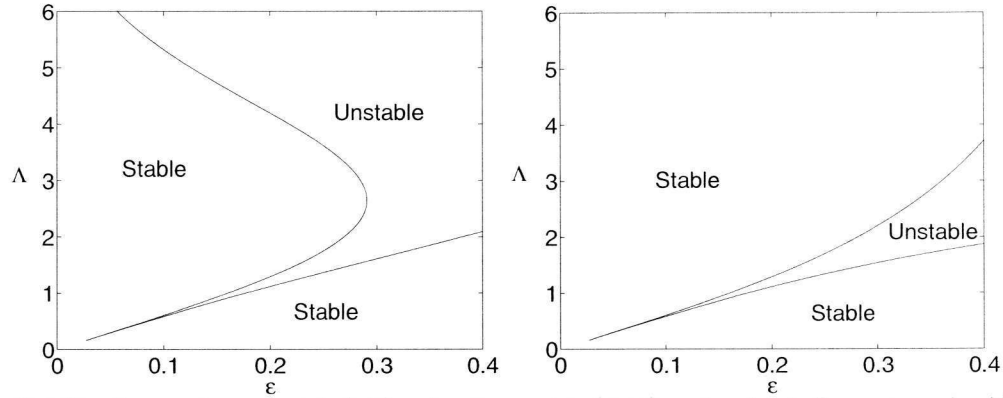

FIG. 3. Stability diagram for symmetric (left) and antisymmetric (right) modes of a similar vortex pair without axial flow: Λ is the wavelength and ε is the initial thickness.

TABLE I. Numerical parameters: open vortices

	Run	Λ	np	dt	nb	nsteps	CPU time*(s)
Straight filament	5	1.25	257	0.00026	8	600	330
Vortex pair period	6	1.25	257	0.00026	8	250	516
Vortex pair growth rate	7	-	101	0.0019	8	800	240
// Non Linear (NL) regime	8	10.21	//	//	//	7950	2520
Four vortices S1 mode	9	0.8976	61	0.0019	20	250	264
// NL regime	10	//	//	//	//	872	930
Four vortices S1 or A mode	11	7.85	101	0.0019	8	250	306
// NL regime	12	//	//	//	//	1744	2160

*SGI R10000 work-station at 225MHz

The period of the symmetric stable modes is [31]

$$T = \frac{4\pi^2 L^2}{\Gamma\sqrt{-(1-\psi+k^2L^2\tilde{\omega})(1+\chi-k^2L^2\tilde{\omega})}}, \tag{2}$$

where $k = 2\pi/\Lambda$ is the wavenumber and

$$\psi = k^2L^2K_0(kL) + kLK_1(kL),$$
$$\chi = kLK_1(kL),$$
$$\tilde{\omega} = (-1 + \log\frac{2}{\delta k} + 1/2 - \gamma + C_v + C_w)/2.$$

Here, K_0 and K_1 are modified Bessel functions of the second kind. The period of the antisymmetric modes is given by [31]

$$T = \frac{4\pi^2 L^2}{\Gamma\sqrt{-(1+\psi+k^2L^2\tilde{\omega})(1-\chi-k^2L^2\tilde{\omega})}}. \tag{3}$$

Figure 4 shows the period T for the wavelength $\Lambda = 1.25$ of the perturbed contra-rotating filaments (symmetric stable modes) as a function of the initial thickness ε. Numerical results (crosses in Fig.4 and Run 6 in Table I) are in excellent agreement with the analytical result (solid line). This period is found in the same way as in Appendix D.3.

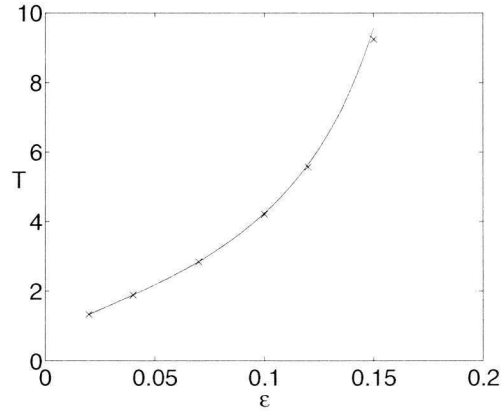

FIG. 4. Period T for the wavelength $\Lambda = 1.25$ of the perturbed contra-rotating vortex pair (symmetric stable modes) versus its initial thickness ε. The solid line is from the analytical result and crosses from numerical computation (Run 6 in Table I).

The growth rate β of the symmetric unstable modes is [31]

$$\beta = \frac{1}{8\pi L^2}\sqrt{(1-\psi+k^2L^2\tilde{\omega})(1+\chi-k^2L^2\tilde{\omega})}. \tag{4}$$

The growing perturbations are planar standing waves with planes fixed at angle θ to the horizontal [31]:

$$\theta = \arctan(\sqrt{(1+\chi-k^2L^2\tilde{\omega})/(1-\psi+k^2L^2\tilde{\omega})}). \tag{5}$$

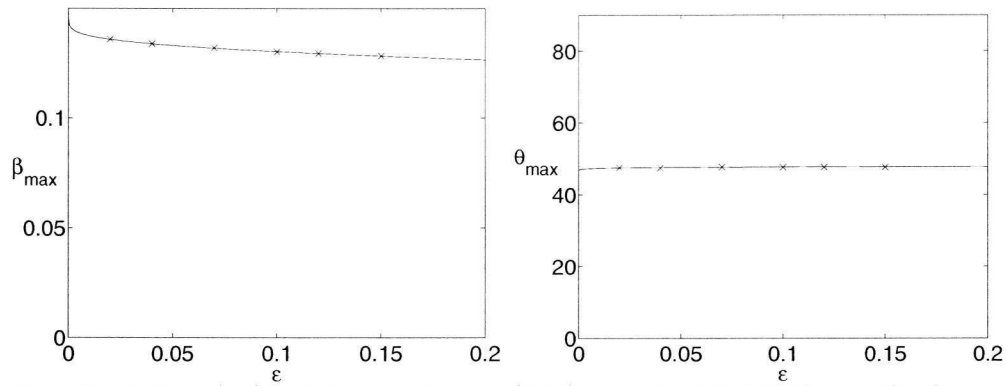

FIG. 5. Growth rate β_{max} (left) and planar angle θ_{max} (right) versus the initial thickness ε for the most unstable wavelength of the perturbed contra-rotating vortex pair (symmetric unstable mode). Same legend as in Fig. 4.

Figure 5 displays the growth rate β_{max} and the planar angle θ_{max} for the most unstable wavelength $\Lambda(\varepsilon)$ (symmetric unstable mode) of the perturbed contra-rotating vortex pair as a function of the initial thickness ε. Numerical results (crosses in Fig. 5 and Run 7 in Table I) are in excellent agreement with the analytical results (solid line). The initial amplitude of the perturbation is $\rho_0 = 0.001$ and the initial planar angle is deduced from (5). It has been checked that the planar angle of the mode did not change during the computation: reported crosses are the value of this angle at the end of the computation. The amplitude $\rho(s,t)$ is given by $\rho^2(s,t) = \left[Z(s,t) - Z(t)\right]^2 + \left[Y(s,t) - 0.5\right]^2$ where $\mathbf{X} = (X,Y,Z)$ and where $Z(t)$ is the spatial average on the

filament at time t. The growth rate is given by the slope of the temporal function $\log[\rho(s,t)/\rho(0)]$. It converges with all numerical parameters (time step, number of points and number of boxes) and with decreasing initial amplitude ρ_0. With an axial flux ($m_0/\Gamma \neq 0$) the ε axis of the previous figures is multiplied by $\exp(-2[m_0/\Gamma]^2)$. We checked that analytical and numerical results also agree for $m_0/\Gamma = 0.6$.

Figure 6 displays the evolution of the Crow instability of the most unstable mode in the non-linear regime (Run 8 in Table I). For sake of clarity the curve of the centerline is represented by a tube with an arbitrary core radius.

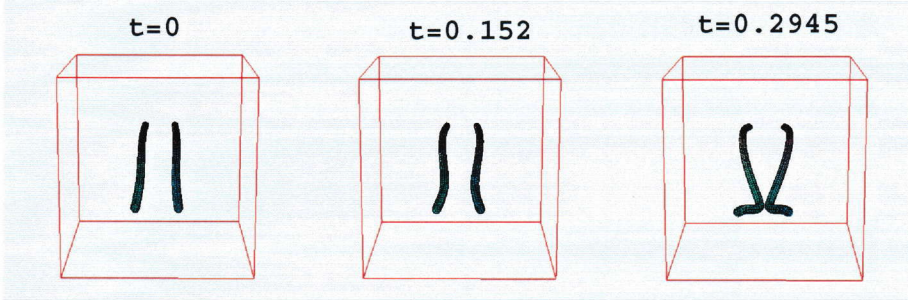

FIG. 6. Vortex Filament Simulation of the non-linear instability regime of the most unstable mode $\Lambda = 10.21$ for the contra-rotating vortex pair. Initial amplitude $\rho = 0.05$, initial thickness $\varepsilon = 0.02$ and initial angle $\theta(t=0) = 47.63(\text{deg})$.

Viscous and non-similar effects are implemented in EZ-vortex but could not be validated by lack of known analytical results. The linear growth rate β found from the first time steps as before is almost constant with the viscous parameter $\bar{\nu} = \nu/\varepsilon^2$ till $\bar{\nu} \simeq 4$. The maximum amplitude on the filament $\rho(t)$ as a function of time is weakly affected by the viscosity ($\bar{\nu} = 1$) in the non-linear regime. The simulations of the Rankine or the *witch-hat* profiles (see Appendix B) give almost the same maximum amplitude $\rho(t)$ evolution as for a similar core.

B. Study of a four-vortex aircraft wake

In this subsection the EZ-vortex code is used to study a four-vortex aircraft wake. It gives a last validation of the code. As in the previous section all following simulations use the M1 de-singularized method of Knio and Klein with the explicit Adams-Bashforth scheme, there is no axial flow ($m_0 = 0$) and the fluid is inviscid ($\bar{\nu} = 0$). Here, the vortex core is a *Rankine* profile. The two trailing vortex pairs have the same axis of symmetry. Let us denote Γ_o, Γ_i, L_o, L_i, $\bar{\delta}_o(t=0)$ and $\bar{\delta}_i(t=0)$ the circulations, the distances and the thickness of the outer and inner vortex pairs. We introduce the dimensionless parameters $R = L_i/L_o$ and $G = \Gamma_i/\Gamma_o$. The initial outer reduced thickness is $\bar{\delta}_o(t=0) = 1$ and so the small parameter ε is the initial thickness of the outer pair.

TABLE II. Four-vortex modes: linear stability (th.) and EZ-vortex (num.) results at $\varepsilon = 0.1$.

	Λ	β	$\theta_o(\text{deg})$	$\theta_i(\text{deg})$	$\varrho = \rho_i/\rho_o$
Most amplified S1 mode (th.) [18]*	0.8976	2.91	105.86	131.24	57.4
// (num. Run 9 in Table I)	//	2.94	111.04	130.20	52.8
Long-wave S1 mode (th.) [18]*	7.85	1.55	145.45	103.85	9.72
// (num. Run 11 in Table I)	//	1.56	145.68	103.73	9.80
Long-wave A mode (th.) [18]*	7.85	1.469	116.90	167.03	9.58
// (num. Run 11 in Table I)	//	1.511	118.72	166.39	9.73

*results given by D. Fabre.

There is an exact stationary solution of the equation of motion (B12) provided that the following relation between G and R is satisfied [20]

$$G = -\frac{3R + R^3}{3R^2 + 1}. \tag{6}$$

The associated velocity V is

$$V = \frac{\Gamma_i}{2\pi L_i} + \frac{2\Gamma_o}{\pi L_o}\frac{1}{1-R^2}. \tag{7}$$

We checked that the EZ-vortex code reproduces this velocity for the ratio $R = 0.14$ (associated G is -0.4.) used by Fabre and Jacquin [18].

As for the contra-rotating vortex pair sinusoidal unstable modes exist. The growing perturbations are planar with planes fixed at angles θ_o (outer trailing pair) and θ_i (inner trailing pair) with respect to the horizontal [18]. Let $\varrho = \rho_i/\rho_o$ be the ratio of the amplitudes. Fabre and Jacquin [18] carried out the linear stability study of this wake and gave results for $R = 0.14$ ($G = -0.4$), $\varepsilon = 0.1$, $\bar{\delta}_o(t = 0) = 1$, $\bar{\delta}_i(t = 0) = 0.5$, $\Gamma_o = 1$ and $L_o = 1$. The growth rates and the associated modes of the most amplified S1 mode $\Lambda = 0.8976$ and for the long-wave S1 and A modes $\Lambda = 7.85$ are given in Table II. We have reproduced these results with the EZ-vortex code by starting from a perturbation amplitude $\rho_0 = 0.001$.

TABLE III. Four-vortex modes: linear stability (th.) at $\varepsilon = 0.02$.

	Λ	β	θ_o(deg)	θ_i(deg)	$\varrho = \rho_i/\rho_o$
Most amplified S1 mode (th.)*	1.2566	3.07	82.81	132.53	48.5
Long-wave S1 mode (th.)*	7.85	1.62	140.36	104.35	10.00
Long-wave A mode (th.)*	7.85	1.40	110.13	167.54	9.35

*results given by D. Fabre.

The growth rate β is obtained from the slopes of the temporal functions $\log[\rho_\alpha(s,t)/\rho_\alpha(0)]$ with the amplitudes $\rho_o(s,t)$ and $\rho_i(s,t)$ measured by

$$\begin{aligned}\rho_o^2(s,t) &= \left[Z_o(s,t) - \bar{Z}_o(t)\right]^2 + \left[Y_o(s,t) - \bar{Y}_o(t)\right]^2,\\ \rho_i^2(s,t) &= \left[Z_i(s,t) - \bar{Z}_i(t)\right]^2 + \left[Y_i(s,t) - \bar{Y}_i(t)\right]^2,\end{aligned} \tag{8}$$

where $\mathbf{X}_\alpha = (X_\alpha, Y_\alpha, Z_\alpha)$ and $\bar{Z}_\alpha(t)$ and $\bar{Y}_\alpha(t)$ are the spatial averages on the filament $\alpha = o$ or i at time t. We start with the linear stability results and carry out several computations starting with $\rho_0 = 0.001$ and with $(\theta_o, \theta_i, \varrho = \rho_i/\rho_o)$ from the final values of previous computation. It converges to fixed values reported in Table II. We have carried out the same comparison for $\varepsilon = 0.02$ and shown that the small difference between numerical and linear stability results disappears (Table III). This difference is thus due to finite ε effects. Figure 7 displays the evolution of these modes in the non-linear regime. The numerical parameters of the computation are given in Table I (Runs 10 and 12).

Most amplified S1 mode $\Lambda = 0.8976$.

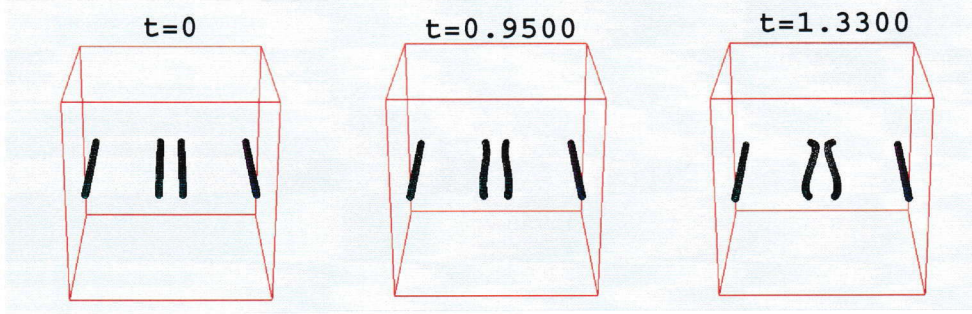

Long-wave S1 mode $\Lambda = 7.85$.

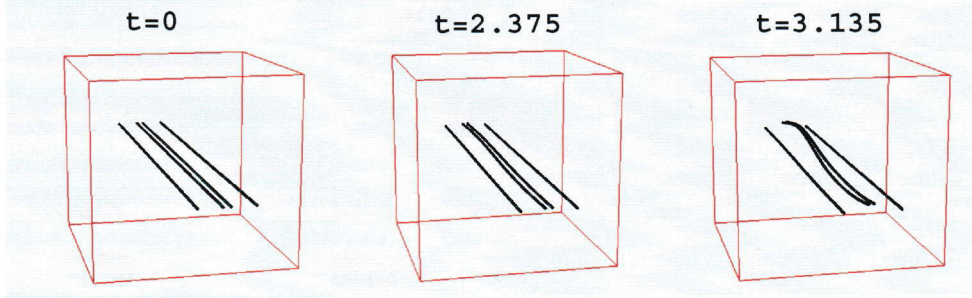

Long-wave A mode $\Lambda = 7.85$.

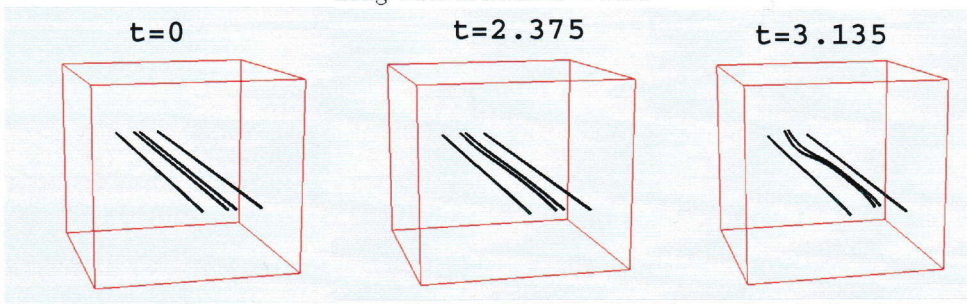

FIG. 7. Vortex Filament Simulation of the non-linear instability regime of typical modes for the four-vortex wake. Initial amplitude $\rho_0 = 0.001$ and initial thickness $\varepsilon = 0.1$. (The visualization of the filaments uses equal core radius even if the computation uses unequal sizes.)

IV. ANALYSE OF WIND TUNNEL DATA

In this section we give a brief overview of the NLR experiments and results in wind tunnel on a generic model: the SWIM model. We then complete the data analysis of NLR to find the physical parameters that we need as an input (initial condition) of our EZ-vortex computation. We first explain how we do the analysis and then give the parameters of the different runs to be done.

A. SWIM geometry and NLR experiments in LST and LLF wind tunnels

These experimental results are for a generic model: the SWIM model geometry, and consist in 6 model configurations. Fig. 8 gives the photos of these 6 configurations and Fig. 9 gives the dimension of the wing and the lateral position of the spoiler elements.

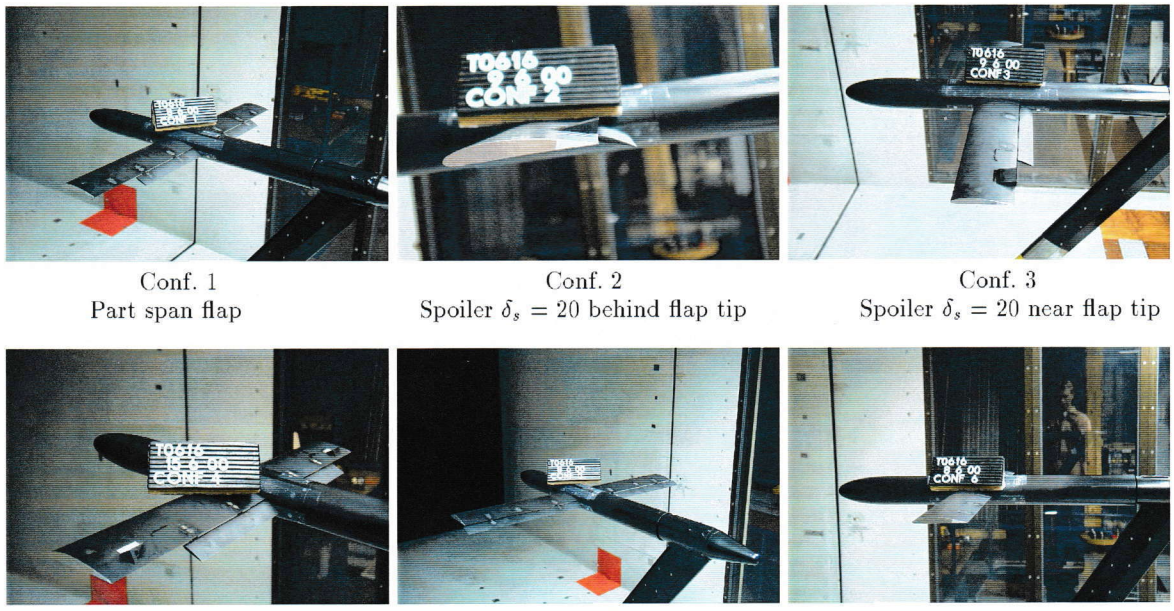

Conf. 1
Part span flap

Conf. 2
Spoiler $\delta_s = 20$ behind flap tip

Conf. 3
Spoiler $\delta_s = 20$ near flap tip

Conf. 4
Spoiler $\delta_s = 20$ near flap tip

Conf. 5
Full span flap

Conf. 6
Clean wing

FIG. 8. The 6 model configurations [25]

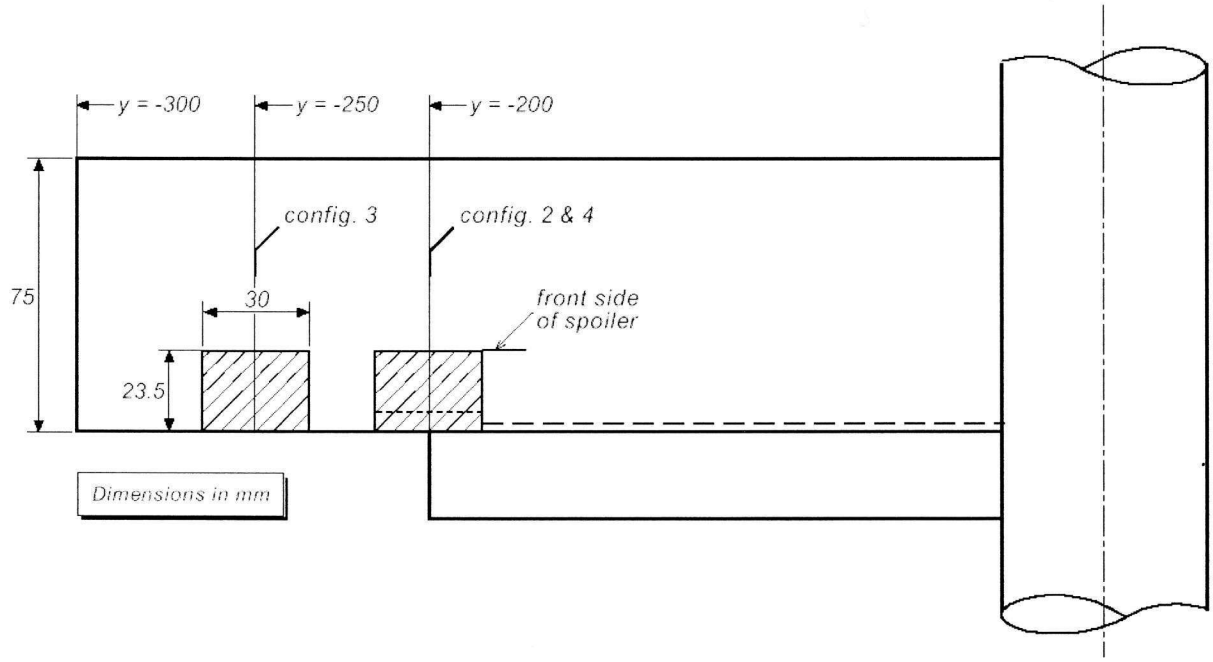

FIG. 9. Wing of the swim model and lateral position of the spoiler elements [14]

The coordinate frame is (x, y, z) where x and z are respectively the down stream and the vertical directions. The associated velocity components are (U, V, W). The wing span is $b = 0.6\ m$ and the mean axial velocity $U_0 = 60\ m/s$. Fig. 10 gives the planning of the different tests in LST and LLf wind tunnels for the different configurations and cross sections. Instrumentation is either PIV or 5-hole rake. The 5-hole rake allows to have the axial component of velocity.

Phase 1 and phase 2 tests in the DNW-LST (phase 1 in italics)							
X position		**Model configuration**					
x/b	[m]	1 (α=6.0 deg)	2 (α=6.9 deg)	3 (α=6.9 deg)	4 (α=7.5 deg)	5 (α=3.5 deg)	6 (α=8 deg)
0.75	0.45	*PIV*	*PIV*	*PIV*	*PIV*	*PIV*	*PIV*
1.25	0.75	Rake/PIV	Rake/PIV	Rake/PIV		Rake/PIV	
2.50	1.50	PIV	PIV	PIV		PIV	
5.00	3.00	*Rake*/PIV	*Rake*/PIV	*Rake*/PIV	*Rake*	*Rake*/PIV	*Rake*
7.50	4.50	PIV					
10.16	6.10	Rake/PIV	Rake/PIV	Rake/PIV		Rake/PIV	
Tests in the DNW-LLF wind tunnel							
10.16	6.10	PIV	PIV	PIV		PIV	
15.33	9.20	PIV	PIV	PIV		PIV	
29.83	17.90	PIV	PIV	PIV		PIV	

FIG. 10. Main flow-field tests in LST and LLF wind tunnels [14]

B. Results and data analysis from NLR

The NLR CD-Rom [25] gives all the results for LST (PIV and Rake) and LLF tests. It consists of different ascii data files. They give the velocity components (over U_0) and the computed axial vorticity component on interpolated grids that cover all the flow field behind the wing. In these files there is a column for each component on the grid. The number of grid points in y and z directions changes from one file to one other and it is not given. In LST measurement PIV results are unable to give the velocity field inside the strongest vortices. For each data file the configuration number and the cross section position x/b can be found from Table 3a to Table 3f in the NLR report [26]. For example Fig. 11 gives the velocity and the vorticity fields that we plot with Matlab from the dat file *rake02022.dat* : rake data results for configuration 1 at $x/b = 5$.

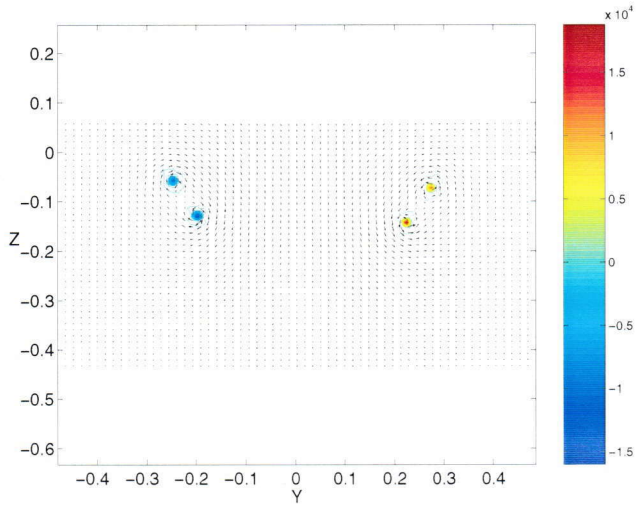

FIG. 11. Velocity field and axial vorticity contourplot for configuration 1 at $x/b = 5$ (file *rake021022.dat* [25])

In order to generate the initial conditions of the EZ-vortex code from these experimental data we need to have a physical analysis of the flow, i.e. to have the physical parameters: *number of vortices, their circulation, position and thickness*. The result of the data analysis of NLR can be found from Table 3a to Table 3f in the NLR report [26]. We can find from these tables the position of vortices and the total circulation on the left and right hand side of the wing. This circulation is found both by a surface integral of the vorticity field (Γ_s) and a line integral of the velocity field (Γ_c). For example for the run of Fig. 11 it gives: $\Gamma_s = -4.125\ m^2/s$ and $\Gamma_c = -4.125\ m^2/s$ on the left hand wing and $\Gamma_s = 3.937\ m^2/s$ and $\Gamma_c = 3.953\ m^2/s$ on the left hand wing. Unfortunately the number of vortices, their individual circulation and their core thickness are not given in these Tables. As we need it we have completed the analysis of NLR by computing these physical parameters for the different experimental data files.

C. Our analysis of the data files

We will present our analysis on the same run as in Fig. 11. We first find the center of the each vortex from Fig. 11 and select a circular domain around its center (Fig. 12).

We then interpolate the vorticity field on a polar grid around this circular domain and do the angular average of this field to obtain the radial velocity profile of vorticity (dot points in Fig. 13). As a Gaussian profile only depends on the circulation Γ and core thickness δ (see Appendix B), these two parameters can been found from an optimization routine to find the Gaussian profile that best fits the experimental one in the least square sense (Fig. 13). We use usual Matlab routines to develop this analyzer of the data files and made this program as automatic as possible. In the same way the amplitude of non-Gaussian moments (in the Laguerre series sense: see Appendix B) can be found.

We find that $\Gamma = -2.7014\ m^2/s$ and $\delta = 0.011\ m$ for the vortex in the circle of Fig. 12. Curiously rake vorticity field are divided by 100 as regard to corresponding PIV-LST vorticity (for example compare files *rake4301.dat* and *piv7501.dat*): we then have multiplied rake vorticity and PIV-LLF vorticity by 100. This procedure of finding the circulation is much more accurate than computing a surface integral of the vorticity

($\Gamma =\sim -3.22\ m^2/s$) or a line integral of the velocity ($\Gamma = -3.5\ m^2/s$). The obtained thickness is also more accurate than the one obtained by using the computed circulation and the extremum of vorticity. The circulation on the left hand wing is $\Gamma = -4.903\ m^2/s$ and the one of the right hand wing is $\Gamma = 5.057\ m^2/s$ to be compared with the values of $\Gamma_s = 4.125\ m^2/s$ and $\Gamma_s = 3.937\ m^2/s$ found by NLR. We also can find the radial profile of $W - U_0$ and extract the axial flux m_0 in the vortex. We find that $M_0/U_0 = -0.00427\ m^2$ for the vortex in the circle of Fig. 12.

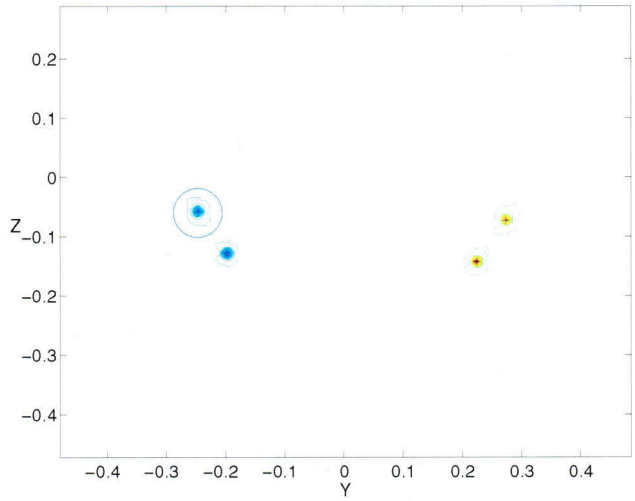

FIG. 12. Contour-plot of vorticity (same data file as Fig. 11). The circle is the domain of analysis of the associated vortex.

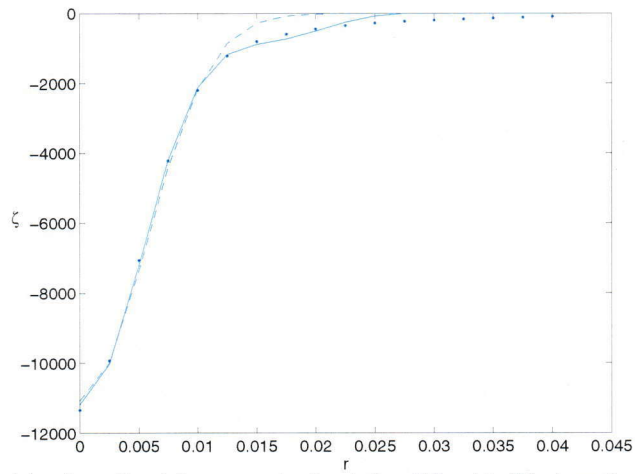

FIG. 13. Radial axial vorticity ζ profile of the vortex in the circle of Fig. 12. We show the experimental profile: dotted line, the best Gaussian profile: dashed line and the best non-Gaussian profile: solid line.

From the analysis of the positions of the vortices we can display the wake of the six configurations (Fig. 14). As can be seen from Fig. 14 there is no long wavelenght 3D effect in these experiments. There is first a merging of the co-rotating filaments with either a 2D merging or a short wavelenght instability merging and then a 2D motion of the resulting trailing vortices. As our code captures 3D curvature long wavelength effect, it is a useful tools to extrapolate these experimental mid field to the far field by using the last cross section velocity field. The last stage $x/b = 30$ of experimental data can be extended to 3D and we can carry out a temporal computation with EZ-vortex. In order to do this we need to extract the physical parameters from the different last cross sections.

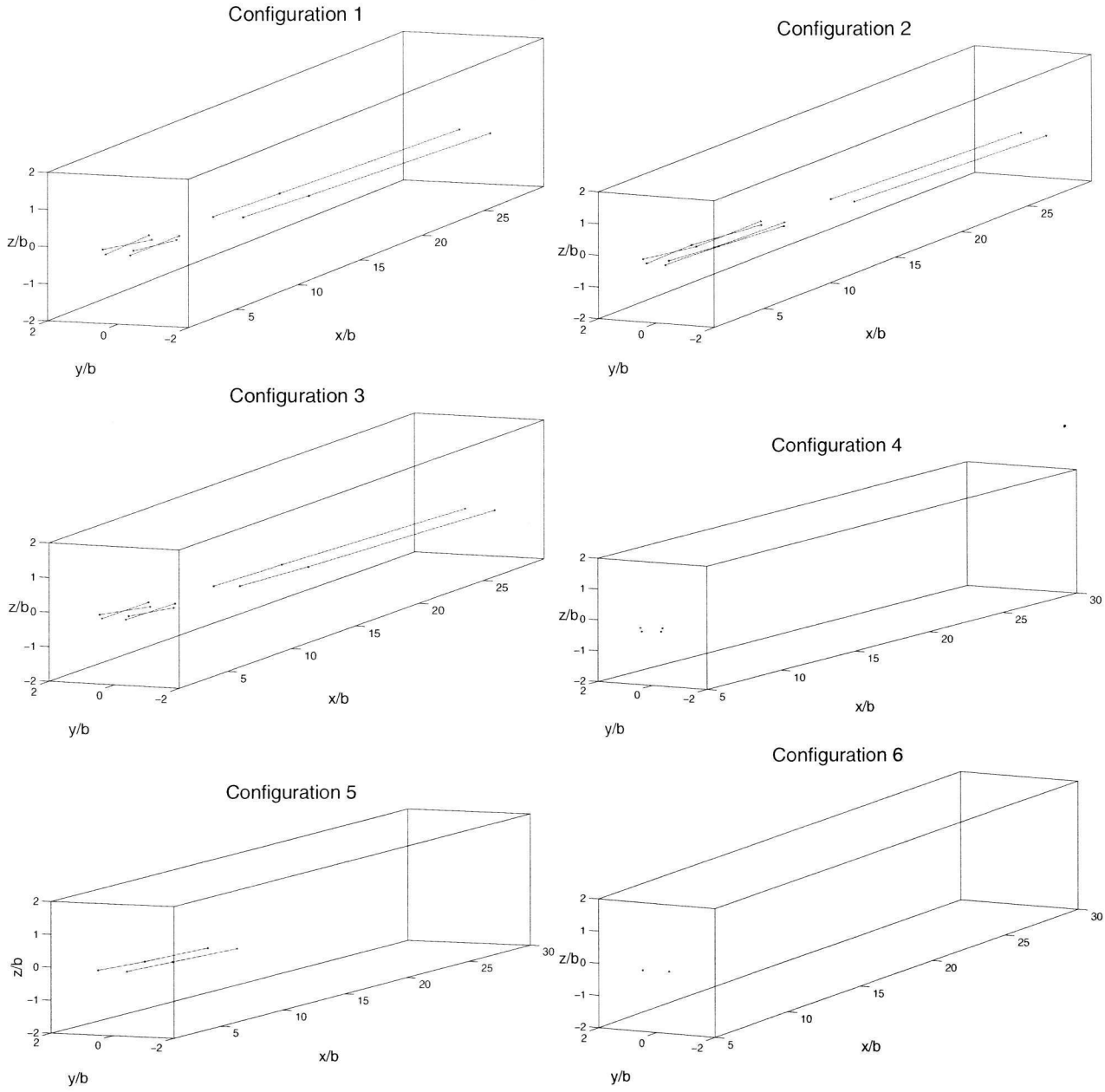

FIG. 14. Position of vortices in the LLS and LLF wind tunnels.

D. The results to be used as EZ-vortex input

The analysis of the different last cross sections gives:

TABLE IV. Positions and characteristics of vortices

Configuration	x/b	y	z	Γ	δ
1	29.83	-0.281	-0.381	-4.107	0.0237
1	29.83	0.245	-0.344	+4.187	0.0236
2	29.83	-0.272	-0.406	-4.358	0.0215
2	29.83	0.243	-0.378	+4.094	0.0235
3	29.83	-0.271	-0.408	-5.467	0.0262
3	29.83	0.218	-0.374	+5.467	0.0262
6	5	-0.260	-0.0475	-2.296	0.00612
6	5	0.280	-0.0625	+2.290	0.00598

In the last cross section of configuration 5 the vortices are still in the merging phase. We have no data files for the last cross section of configuration 4. The last section of configuration 6 is at $x/b = 5$. For these reasons *we will use the last section of configuration 1, 2, 3 and 6.*

The last stage $x/b = 30$ of experimental data is extended to 3D and we carry out a temporal computation with this initial condition. We recall that the Wing span is $b = 0.6\ m$ and the axial mean velocity is $U_0 = 60\ m/s$. The physical parameters of the computation are : the circulation Γ, the core radius aspect ratio $\varepsilon = \delta/L$ (where L is the distance of vortices), the reduced viscosity $\nu = \nu/\varepsilon^2 = 15.69\ 10^{-6}/\varepsilon^2\ (m^2/s)$ and the axial flux m_0. The axial flux m_0 of the theory is related to the experimental axial flux M_0 by $m_0 = M_0/\varepsilon(m^3/s)$. As we have no results for the axial flux in the last section we will assume $m_0 = 0$. From Table IV we can find the remaining parameters of the simulations (Table V).

TABLE V. Physical parameters of the simulations

Configuration	$\Gamma\ (m^2/s)$	L (m)	ε	$\bar{\nu}\ (m^2/s)$
1	$\pm$ 4.15	0.527	0.0460	0.0077
2	$\pm$ 4.23	0.516	0.0436	0.0082
3	$\pm$ 5.47	0.490	0.0530	0.0056
6	$\pm$ 2.29	0.540	0.0112	0.1290

The small core radius aspect ratio ε is coherent with the slenderness assumption.

V. PARAMETRIC STUDY WITH EZ-VORTEX

The last stage $x/b = 30$ of experimental data is extended to 3D and we carry out a temporal computation with this initial condition. The computation is stopped at the collision time t_c defined with the criteria of collision $d_{min}/L = 4\varepsilon$ where d_{min} is the minimal distance between the vortices.

The linear symmetric mode characteristics are given in Table VI

TABLE VI. Linear mode characteristics.

Configuration	Λ (m)	θ (degre)	β (1/s)
1	4.8336	47.61	1.992
2	4.7653	47.50	2.124
3	4.7673	47.61	3.028
6	5.8482	47.39	1.078

where Λ is the wavelength, θ the planar angle and β the growth rate of the most unstable mode. We checked that EZ-vortex gives these growth rates in the linear regime for the 4 configurations.

The numerical parameters of the computations are given in Table VII.

TABLE VII. Numerical parameters: open vortices

Configuration	Λ	np	dt (s)	nb	nsteps	CPU time*(s)
1	4.8336	101	0.000285	8	7950	2542
2	4.7653	101	0.000285	8	7950	2551
3	4.7673	101	0.000285	8	7950	2558
6	5.8482	151	0.00038	8	11925	8548

*SGI R10000 work-station at 225MHz

The linear time is $t_l = 1/\beta$ where β is the linear growth rate. The result of the computations is given in Table VIII, where $t^* = t/t_0$ with $t_0 = 2\pi L^2/\Gamma$ [2].

TABLE VIII. Linear and collision times ($\rho_0 = 0.01$ (m), *i.e.* $\rho_0/L \sim 0.02$).

Configuration	t_0 (s)	t_l (s)	t_l^*	t_c (s)	t_c^*
1	0.42	0.50	1.19	1.67	3.97
2	0.39	0.47	1.21	1.55	3.98
3	0.27	0.33	1.22	1.14	4.22
6	0.8	0.93	1.16	3.04	3.8

Numerical computation of configurations 1, 2, 3 and 6 are given in Fig. 15-18.

Configuration 1

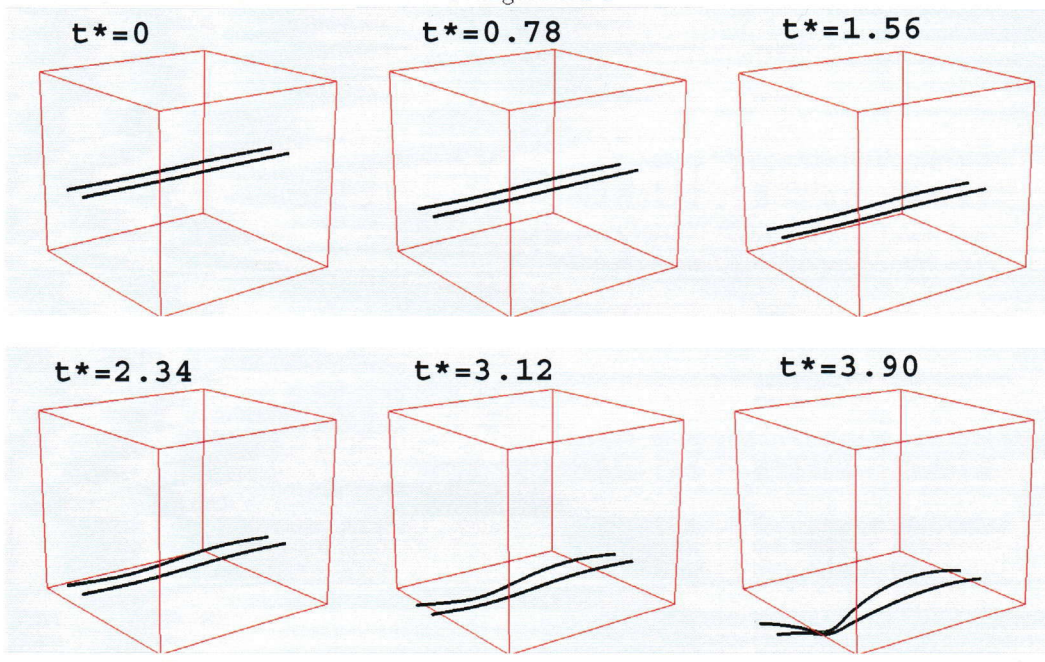

FIG. 15. Vortex Filament Simulation of the far wake for configuration 1.

Configuration 2

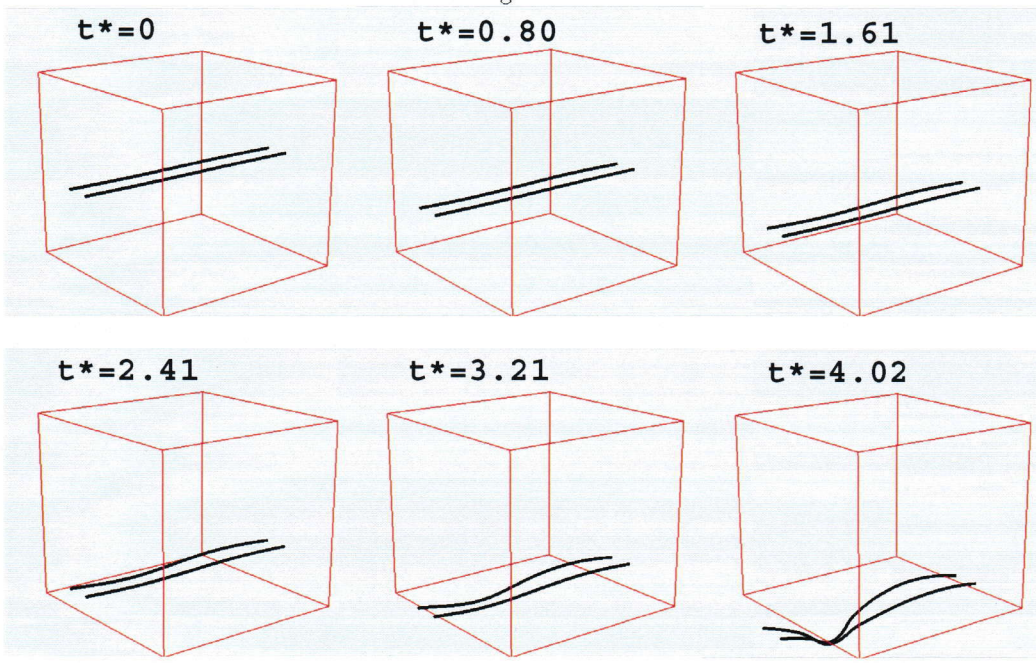

FIG. 16. Vortex Filament Simulation of the far wake for configuration 2.

Configuration 3

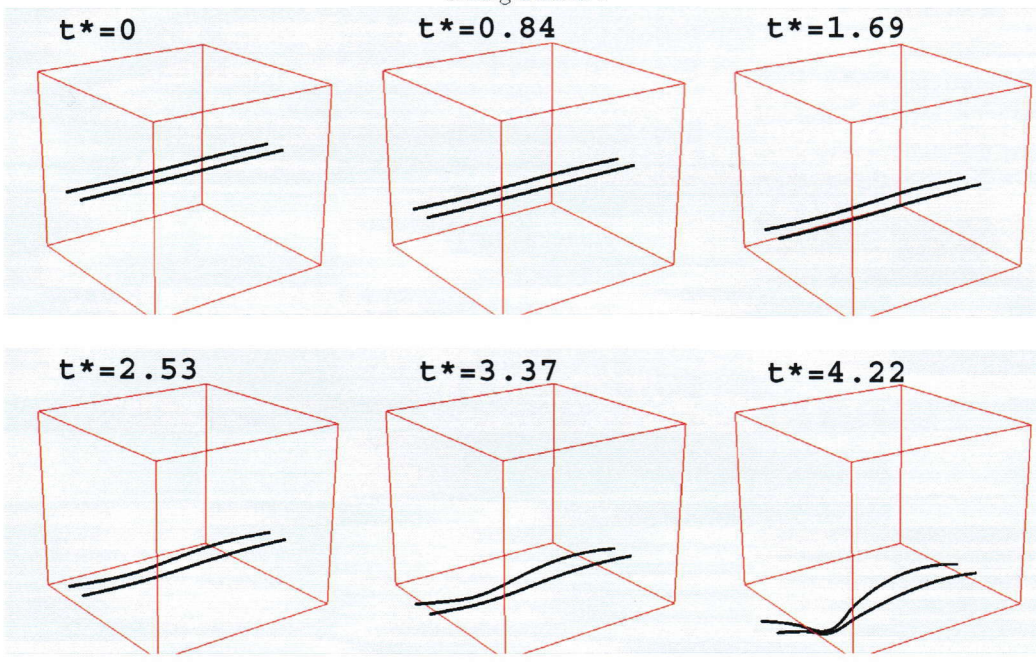

FIG. 17. Vortex Filament Simulation of the far wake for configuration 3.

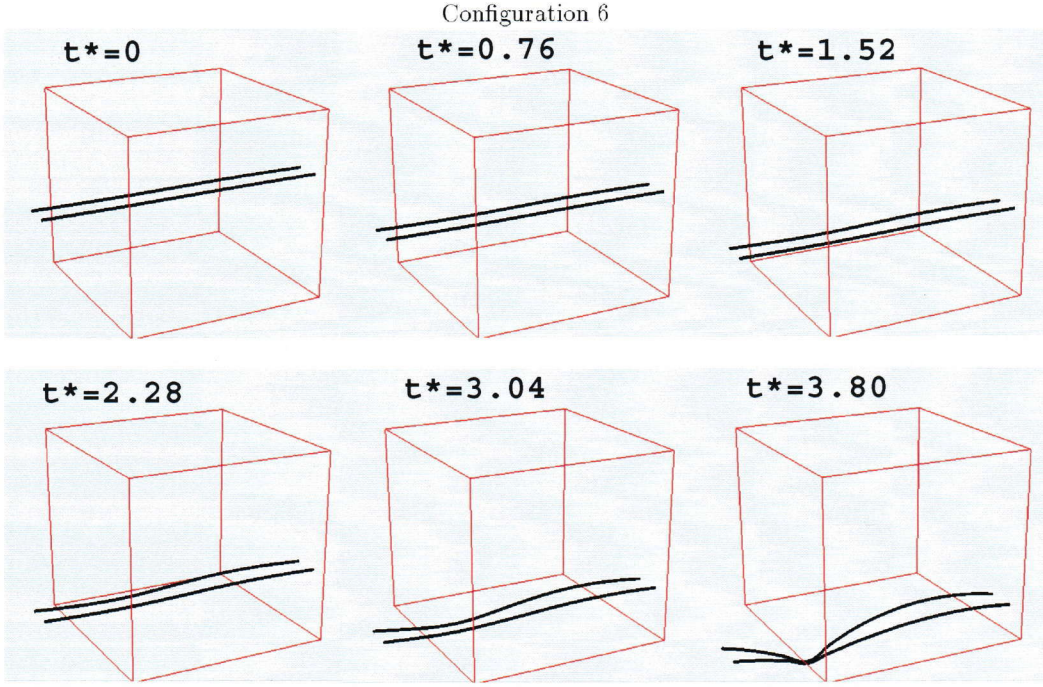

FIG. 18. Vortex Filament Simulation of the far wake for configuration 6.

Our main conclusions for this parametric study are as follow:

- For the 4 configurations the collision time is about 3.3 times the linear stability time ($t_c \equiv 3.3t_l$).
- In dimensionless form all simulations and collision time are almost the same.
- In dimension form configuration 3 is the quickest to reconnect the vortices.

VI. CONCLUSION AND PERSPECTIVES

A code EZ-vortex has been developed to compute the motion of slender vortex filaments of closed or open shape. The implemented equation is the M1 de-singularized method of Knio and Klein but other equivalent equations are also implemented as a useful comparison. The fluid may be inviscid or not, the vortex core is similar or not, and there can be an axial flow or not. The validity of all these equations are based on the Callegari and Ting asymptotic results. The advantages of the different formulations and discretizations of the associated equations are discussed. The philosophy of EZ-Vortex code is to keep programs as simple as possible and to provide documentation both by way of a text and comments within the code itself. It will be available through the world-wide web.

This code has been validated against known solutions of these equations and results of linear stability studies. The linear and non-linear stages of a perturbed two-vortex wake and of a four-vortex wake model have been studied till the reconnection phase, which is outside the validity of the asymptotic analysis and of the associated integro-differential equations. In the linear phase the comparison with analytical stability results is excellent. We give the optimal values of the numerical parameters that give converged results with the code.

The experimental data from NLR in the near- and mid- field have been further analysed to give the physical parameters needed as an input in our code. The vortex filament thickness was not given in the NLR analysis of their data and is an essential parameter to give accurate 3D simulations which take into account 3D curvature effects. In these experiments the vortex core appears to be slender and there are no 3D long wavelength effect in the experimental wake. The last cross section is used to do a parametric study of the far wake.

Our main results and conclusions are as follow:

- The EZ-vortex code is the implementation of a Slender Vortex Method and is very good tool to compute the far wake up to the long wavelength reconnection phase.
- It includes large axial velocity and non-similar profiles in the vortical cores. The fluid may be viscous or inviscid.
- It does not include short wavelength, merging and reconnection.
- It has been validated against linear stability results.
- It is very easy to handle; a documentation and typical parameters of convergence are given.
- It is the only *fast* computation code of the far field.
- It allowed us to compute temporal evolution of the far field from wind tunnel results provided that the physical parameters of the experimental data in the last wind tunnel cross section are given.
- It needs to be coupled with near- and mid- field results to do a parametric study with the wing parameters as an input.
- It was used to do a parametric study by extended to 3D the last stage $x/b = 30$ of LST and LLF wind tunnels and running a temporal computation.

Our main perspectives are as follow:

- It may be a useful tool to compute the far wake (up to the reconnection phase) and may be used to compare far field experimental data from catapult, tower tank or flight measurements in real atmosphere.
- Simple reconnection models [32–34] may be also implemented to go through the reconnection phase.
- A fast engineering code (in the same idea as the 2D code of Corjon [35]) could be developed from this code by adding 3D models of reconnection so that to continue the computation through the trailing pair reconnection.
- It is straightforward to add an potential background flow (*i.e.* lateral wind).
- It could be adapted to do spatial computation, *i.e* computation in a frame attached to the plane rather than attached to the ground. Such kind of computation was used by Saghbini *et al.* [36] to study vortex breakdown.
- It may be used to study other non-stationary four-vortex wake configurations as the one studied in the linear regime by Crouch [37] or the non-linear stage of two rotating vortices of different circulations.

- The higher order asymptotic result obtained by Margerit [38] may be implemented in order to get higher order results, *i.e* thicker vortex core, and to offer the possibility of a quantitative comparison with a direct numerical simulation of the Navier-Stokes equations.

It is recommended that EZ-vortex is used to develop an engineering fast computation code and to give a comparison between numerical simulation and far field experimental data from catapult, tower tank or flight measurements in real atmosphere. A comparison with far field LES computations would be also of interest.

It should be noted that a paper that describes the code and its validation has been submitted to Int. J. of Numer. Meth. in Fluids [9].

APPENDIX A: THE DIFFERENT VORTEX METHODS AND THEIR CHARACTERISTICS

In this appendix we give a brief overview of different *vortex methods* and we explain the interest of *slender vortex methods.*

Vortex Methods are characterized by the following three features. i) The underlying discretization is of the vorticity field, rather than the velocity field. Usually this discretization is Lagrangian in nature and frequently it consists of a collection of particles or of filaments which carry concentrations of vorticity. ii) An approximate velocity field is recovered from the discretized vorticity field via the Biot-Savart law. iii) The vorticity field is then evolved in time according to this velocity field.

Among the different vortex methods [5] which have the above features, one can distinguish 'Vortex Blob Methods' and 'Vortex Filament Methods'. In Vortex Blob Methods the vorticity field is discretized by overlapping blobs of vorticity and an equation is used to evolve in time the *local strength* of each blobs in order to take into account the stretching of the vorticity field. In Vortex Filament Methods the vorticity field is discretized by overlapping filaments and the stretching is automatically accounted for by the movement of discretized points on the filament in relation to one another. In these two methods the viscosity may be taken into account by a random walk or a deterministic technique. The Biot-Savart computation of the velocity induced by the discretized field of N blobs or N bits of filaments leads to a N-body problem. The cost of this computation may be diminished by so called 'fast solver' that use different tricks : multi-pole expansion for the far field, numerical evaluation of a Poisson's equation on a fixed grid (the Vortex-in-Cell method),... In the literature there are proofs of the convergence of some of these numerical scheme to the Euler or the Navier Stokes equation in 2D or 3D.

From the point of view of perturbation methods Callegari and Ting [10] have derived an equation of motion for the centerline of 'slender' vortex filaments from the Navier Stokes equations thanks to a matched asymptotic expansion in terms of the thickness of the filament. We call 'slender vortex filament methods' the class of numerical methods which are based on the numerical discretization of this equation. These methods are inviscid or viscous and have the advantage to be derived from the Navier Stokes equations. In these methods the thickness of the filaments has to be small, they do not take into account short waves [39] and the distance between two filaments has to be greater than their thickness and so these methods do not allow reconnection of vorticity. Let us recall that a *slender vortex ring* of circulation Γ is a field of vorticity which is non-zero only in the neighbourhood of a three-dimensional curve $\mathcal{C}$, called the *centerline*. This curve is described parametrically by a function $\mathbf{X} = \mathbf{X}(s,t)$ which denotes a point on the curve as a function of the parameter s, with $s \in [-\pi, \pi[$, and the time t. The thickness δ of the ring is of order l and the other length scales, for example the local *curvature* K or the length S of $\mathcal{C}$, are of the same order L. Since the vortex is slender, a small parameter $\varepsilon \ll 1$ is defined as the ratio l/L. Using a careful matched asymptotic expansion in the Navier-Stokes equations, Callegari and Ting [10] found the following equation of motion

$$\partial \mathbf{X}/\partial t = \mathbf{Q} + \frac{K(s,t)}{4\pi}\left[-\log\varepsilon + \log(S) - 1 + C_v(t) + C_w(t)\right]\mathbf{b}(s,t), \tag{A1}$$

where $\mathbf{Q} = \mathbf{A}(s,t) - [\mathbf{A}(s,t)\cdot\mathbf{t}(s,t)]\,\mathbf{t}(s,t)$ with

$$\mathbf{A}(s,t) = \frac{1}{4\pi}\int_{-\pi}^{+\pi} \sigma(s+s',t)\left[\frac{\mathbf{t}(s+s',t)\times(\mathbf{X}(s,t)-\mathbf{X}(s+s',t))}{|\mathbf{X}(s,t)-\mathbf{X}(s+s',t)|^3} - \frac{K(s,t)\mathbf{b}(s,t)}{2\,|\lambda(s,s',t)|}\right]\mathrm{d}s',$$

and $\lambda(s,s',t) = \int_{s}^{s+s'} \sigma(s^*,t)\mathrm{d}s^*$. Here the velocity field is non-dimensionalized by Γ/L and all lengths by L. In this Equation (A1), $C_v(t)$ and $C_w(t)$ are known functions [10] which describe the orthoradial and axial evolution of the inner velocity in the core. This Equation (A1) holds for a vortex ring with axisymmetric structure at leading order and no axial core variation at this order.

Let us recall that the induced velocity of a curved vortex filament of zero thickness, *i.e.* a line vortex, near its centerline is known to have a binormal component proportional to its curvature and to the logarithm of the distance to the centerline [40,41]. The induced velocity on the centerline is thus infinite and this line vortex model is not the leading-order part of the expansion of a *slender* vortex filament in terms of its thickness. From the point of view of perturbation methods the *slender* filament corresponds to a boundary layer near its moving centerline. The original Navier-Stokes equations are then stiff to be solved numerically. By using a matched asymptotic expansion in terms of the filament thickness Callegari and Ting [42,10,32] have derived an equation of motion for the centerline from the Navier-Stokes equations. SVF are numerical methods which are based on the numerical discretization of this equation [43].

Previous to this matched asymptotic derivation several ad-hoc desingularizations of the Biot-Savart self-induction of a line vortex were proposed [44]. These methods introduce an ad-hoc *parameter of desingularization* to take care of the finite thickness of the filament. In *the cut-off method* [31,45] the desingularization is obtained by cutting a neighborhood of the induced velocity point in the Biot-Savart self-induction of a line vortex: the introduced *cut-off length* is the ad-hoc parameter of desingularization. This cut-off method was used in most stability studies of slender vortex filaments [31,46]. For example, with the cut-off integral technique [31,45] an ad-hoc cut-off of the line integral (A2)

$$\mathbf{v}(r,\varphi,a) = \frac{1}{4\pi}\int_{\mathcal{C}} \frac{\mathbf{t}(a')\times(\mathbf{x}-\mathbf{X}(a'))}{|\mathbf{x}-\mathbf{X}(a')|^3}\mathrm{d}a', \tag{A2}$$

gives a de-singularization of this integral in terms of the distance r to this line and yields the equation of motion:

$$\partial\mathbf{X}/\partial t = \frac{1}{4\pi}\int_{I} \sigma(s',t)\frac{\mathbf{t}(s',t)\times(\mathbf{X}(s,t)-\mathbf{X}(s',t))}{|\mathbf{X}(s,t)-\mathbf{X}(s',t)|^3}\mathrm{d}s', \tag{A3}$$

where $I = [0,2\pi[\backslash[s-s_c, s+s_c[$ and s_c is an unknown small parameter called the *cut-off length*. This integral (A3) is *singular* in terms of the small parameter s_c and can be expanded in terms of this parameter.

By a direct comparison between such ad-hoc equations of motion and asymptotic equation of motion Widnall *et al.* [47,48] and then Moore and Saffman [49,41] give the relation between the cut-off length and the inner structure of the filament. More recently Margerit *et al.* [21] did the comparison with the Callegari and Ting equation. With this relation the cut-off line-integral equation of the centerline is equivalent to Callegari and Ting equation. The comparison between the expansion in s_c of A3 and (A1) leads to

$$s_c(s,t) = \frac{\varepsilon}{2\sigma(s,t)}\exp\left(1-C_v(t)-C_w(t)\right). \tag{A4}$$

This gives the relation between the cut-off length s_c, the reduced thickness ε and the inner-core parameters $C_v(t)$ and $C_w(t)$ of Callegari and Ting. So Equations (A3–A4) are equivalent to Equation (A1), except that, when s_c of (A4) is plugged into (A3), the integral is singular in terms of ε, while the integral $\mathbf{A}$ in (A1) is not. This comparison can be done with other ad-hoc desingularisation methods. The numerical discretization of these equations gives other Slender Vortex Filament methods. However, the resulting justified desingularization methods are still stiff to be solved numerically as the Biot-Savart desingularized integral of these methods is a singular integral in the parameter of desingularization: the centerline in the neighborhood of any point on the filament is a boundary layer for the induced velocity contribution at this point and so needs extra discretized elements.

Vortex Filament methods discretize the field of vorticity by a bunch of overlapping filaments. The velocity induced by a singular vortex filament $\mathcal{C}$ of vorticity

$$\boldsymbol{\omega} = \delta_{\mathcal{C}}\mathbf{t} \equiv \int_{\mathcal{C}} \delta(\mathbf{x}-\mathbf{X}(a'))\mathbf{t}(a')\mathrm{d}a', \tag{A5}$$

is

$$\mathbf{v} = (K(\mathbf{x})\times) * \delta_{\mathcal{C}}\mathbf{t} \equiv \int_{\mathcal{C}} K(\mathbf{x}-\mathbf{X}(a'))\times\mathbf{t}(a')\mathrm{d}a', \tag{A6}$$

where

$$K(\mathbf{x}) = -[1/(4\pi)]\mathbf{x}/|\mathbf{x}|^3. \tag{A7}$$

As the velocity on the filament is singular, Vortex Filament Methods introduce a de-singularization parameter σ, such that the velocity induced by a regularized vortex filament of vorticity

$$\boldsymbol{\omega}_\sigma = f_\sigma(\mathbf{x}) * \delta_{\mathcal{C}}\mathbf{t} \equiv \int_{\mathcal{C}} f_\sigma(\mathbf{x}-\mathbf{X}(a'))\mathbf{t}(a')\mathrm{d}a', \tag{A8}$$

is

$$\mathbf{v}_\sigma = (K_\sigma(\mathbf{x})\times) * \delta_{\mathcal{C}}\mathbf{t} \equiv \int_{\mathcal{C}} K_\sigma(\mathbf{x}-\mathbf{X}(a'))\times\mathbf{t}(a')\mathrm{d}a', \tag{A9}$$

where

$$K_\sigma(\mathbf{x}) = K * f_\sigma(\mathbf{x}) = -g_\sigma(\mathbf{x})\mathbf{x}/|\mathbf{x}|^3, \tag{A10}$$

with

$$f_\sigma(\mathbf{x}) = f(|\mathbf{x}|/\sigma)/\sigma^3, \tag{A11}$$

$$g_\sigma(\mathbf{x}) = g(|\mathbf{x}|/\sigma). \tag{A12}$$

Here f is a function such that $4\pi \int_0^\infty f(r)r^2 \mathrm{d}r = 1$ and $g(r) = \int_0^r f(\xi)\xi^2 \mathrm{d}\xi$. The bunch of vortex filaments is evolved with the induced velocity (A9) and a diffusion step can be superimposed. Vortex Blob methods are similar but use an added dynamic equation for the evolution of the strength of each vortex blobs. Instead of computing the velocity field from (A9) Vortex in Cells (VIC) methods solve the Poisson's equation

$$\nabla^2 \boldsymbol{\psi}_\sigma = -\boldsymbol{\omega}_\sigma, \tag{A13}$$

where $\boldsymbol{\psi}_\sigma$ is the potential vector such that $\mathbf{v}_\sigma = \nabla \times \boldsymbol{\psi}_\sigma$. In these methods fast poisson solver can be used.

By using the Callegari and Ting equation Klein and Knio [11] have shown that it is not correct to compute a vortical flows composed of several thin vortex filaments by a standard VF method [5] with only one *numerical filament* per section of vortex (the so called thin-tube model): more than one numerical filament per section is needed to insure the convergence of the numerical scheme. However, as it would save computation time to have only one numerical filament per section Klein and Knio [11] proposed a cure: they have shown how to adjust the numerical desingularization parameter (the so called thin-tube thickness) to physical thickness of the slender vortex filaments so that the method is correct. This corrected method is based on a comparison with the Callegari and Ting equation of motion and gives another Slender Vortex Filament method. As for the justified desingularization methods and for the same reason, the resulting corrected thin-tube model is still stiff to be solved numerically. This stiffness of the corrected method is now removed in the *improved thin tube models* proposed by Knio and Klein [12].

APPENDIX B: THE GOVERNING EQUATIONS

In this appendix we give the integro-differential equations governing the motion of the centerline that we have implemented in the EZ-vortex code. They are either the Callegari and Ting equations, which are the leading order solution of a matched asymptotic analysis [10], or a simple de-singularized method, or the M1 de-singularized method of Knio and Klein [11,12]. Even if these equations are equivalent their discretized form may be more or less advantageous from the point of view of their numerical stability or of the simplicity of their implementation as shown in Sec. II. For its historical interest the Local Induction Model (LIA) has also been implemented even if it is not equivalent to the previous equations.

1. The Callegari and Ting equation of a closed filament

The Callegari and Ting equation is [10]

$$\partial \mathbf{X}/\partial t = \frac{\Gamma K(s,t)}{4\pi}\left[-\log\varepsilon + \log(S) - 1 + C_v(t) + C_w(t)\right]\mathbf{b}(s,t) + \mathbf{A}(s,t), \tag{B1}$$

where $\mathbf{X}(s,t)$ is the centerline of the filament at time t, $s \in [-\pi,\pi[$ being a parameter on the filament; Γ is its circulation and K is the local curvature. The small parameter ε is the asymptotic parameter of the expansion and corresponds to the aspect ratio δ/L, where δ is the radius of the vortex core and L a typical longitudinal length. S is the length of the closed filament, $(\mathbf{t},\mathbf{n},\mathbf{b})$ is the Frenet frame of the curve $\mathbf{X}$, and $C_v(t)$ and $C_w(t)$ are known functions that depend on the orthoradial and axial evolution of the inner velocity in the core. Here, $\mathbf{A}(s,t)$ is the non-local self-induction of the filament and is given by

$$\mathbf{A}(s,t) = \frac{\Gamma}{4\pi}\int_{-\pi}^{+\pi}\sigma(s+s',t)\left[\frac{\mathbf{t}(s+s',t)\times(\mathbf{X}(s,t)-\mathbf{X}(s+s',t))}{|\mathbf{X}(s,t)-\mathbf{X}(s+s',t)|^3} - \frac{K(s,t)\mathbf{b}(s,t)}{2\,|\lambda(s,s',t)|}\right]\mathrm{d}s',$$

where $\sigma(s,t) = |\partial\mathbf{X}/\partial s|$, and $\lambda(s,s',t) = \int_s^{s+s'}\sigma(s^*,t)\mathrm{d}s^*$.

2. The core-structure functions $C_v(t)$ and $C_w(t)$

The velocity field in the core is described by introducing the *local curvilinear coordinate system* $\mathbf{M}(r,\varphi,s)$ and the curvilinear vector basis $(\mathbf{e}_r,\mathbf{e}_\varphi,\mathbf{t})$. This system is defined in the following manner; if $\mathbf{P}(s)$ is the projection on the centerline $\mathbf{X}$ of a point $\mathbf{M}$ near the curve then $\mathbf{PM}$ is in the plane $(\mathbf{n},\mathbf{b})$ and thus polar coordinates (r,φ) can be used in this plane with the associated polar vectors $(\mathbf{e}_r,\mathbf{e}_\varphi)$. In the asymptotic theory [10] the relative velocity $\mathbf{V}$ is defined by $\mathbf{v} = \partial\mathbf{X}/\partial t + \mathbf{V}$ where $\mathbf{v}$ is the fluid velocity. We denote by (u,v,w) the radial, circumferential and axial components of $\mathbf{V} = u\mathbf{e}_r + v\mathbf{e}_\varphi + w\mathbf{t}$.

The expressions of the core-structure functions $C_v(t)$ and $C_w(t)$ are different depending on the initial leading-order velocity profiles in the core and on the viscosity of the fluid. In this subsection we successively give the velocity profiles and the core-structure functions $C_v(t)$ and $C_w(t)$ for an inviscid, similar and non-similar vortex core.

a. Inviscid vortex core

If the fluid is inviscid the leading-order circumferential and axial components of the relative velocity field are in the form [32]

$$v(r,t) = v_0(r/\delta)\left[S_0/S(t)\right]^{-1/2},$$
$$w(r,t) = w_0(r/\delta)S_0/S(t),$$

where $r = r/\varepsilon$ is the stretched radial distance to the filament, $\delta = \delta/\varepsilon$ is the stretched radius, $[v_0(\eta = r/\delta_0), w_0(\eta = r/\delta_0)]$ is the initial velocity field, and S_0 is the initial length of the filament. The ε-stretched radius δ is

$$\delta^2(t) = \delta_0^2 S_0/S(t).$$

The inner functions are given by [32]

$$C_v(t) = C_v(0) - \log\delta(t),$$
$$C_w(t) = C_w(0)\left[S_0/S(t)\right]^3,$$

where $C_v(0)$ and $C_w(0)$ are the associated initial core constants.

b. Similar vortex core

The circumferential and axial components of the relative velocity field for a similar vortex are [32]

$$v(r,t) = \frac{\Gamma}{2\pi r}\left[1 - e^{-(\bar{r}/\delta)^2}\right], \qquad w(r,t) = \frac{m_0}{\pi\delta^2}\left(\frac{S_0}{S}\right)^2 e^{-(\bar{r}/\delta)^2},$$

where r and δ are defined as before, and m_0 is the initial axial flux of the vortex. The stretched radius δ is given by [32]

$$\delta^2(t) = \delta_0^2\left[\frac{S_0}{S(t)}\right]1_{\bar{\nu}}$$
$$1_{\bar{\nu}} = 1 + \frac{\delta_{\bar{\nu}}^2}{\delta_0^2},$$
$$\delta_{\bar{\nu}}^2 = 4\nu\int_0^t \frac{S(t')}{S_0}\mathrm{d}t',$$

where $\nu = \nu/\varepsilon^2$ is the stretched kinematic viscosity of the fluid of kinematic viscosity ν. The inner functions are given by [32]

$$C_v(t) = (1 + \gamma - \ln 2)/2 - \ln(\delta),$$
$$C_w(t) = -2(S_0/S)^4\left[m_0/(\Gamma\delta)\right]^2,$$

where γ denotes Euler's constant. The effect of the diffusion is easily seen in these expressions through $\delta_{\bar{\nu}}$ (the diffusion-added ε-stretched thickness of the core) in δ and the influence of the stretching through the ratio S_0/S. The inviscid-similar vortex corresponds to $\nu = 0$.

c. Non-similar vortex core

If the flow is viscous ($\nu \neq 0$) and the core is non-similar, the circumferential and axial components of the relative velocity field are in the form

$$v(r,t) = \frac{1}{\eta\delta}\left[\frac{\Gamma}{2\pi}\left(1 - \mathrm{e}^{-\eta^2}\right) + \mathrm{e}^{-\eta^2}\sum_{n=1}^{\infty}\delta_0^2 D_n P_n(\eta^2)1_{\bar{\nu}}^{-n}\right],$$
$$w(r,t) = \frac{2}{\delta^2}\left[\frac{S_0}{S(t)}\right]^2\left[\frac{m_0}{2\pi}\mathrm{e}^{-\eta^2} + \mathrm{e}^{-\eta^2}\sum_{n=1}^{\infty}\delta_0^2 C_n L_n(\eta^2)1_{\bar{\nu}}^{-n}\right],$$

where $\eta = r/\delta$ and the stretched radius δ expression is the same as for a similar vortex. Here, L_n are the Laguerre polynomials, $P_n(\eta^2) = L_{n-1}(\eta^2) - L_n(\eta^2)$, and (C_n, D_n) are the Fourier components of the initial axial velocity w_0 and tangential vorticity $\zeta_0 = [\partial(rv_0)/\partial r]/r$:

$$C_n = \int_0^{\infty} w_0(\eta)L_n(\eta^2)\eta\mathrm{d}\eta,$$
$$D_n = \int_0^{\infty} \zeta_0(\eta)L_n(\eta^2)\eta\mathrm{d}\eta.$$

In particular we have $C_0 = m_0/2\pi\delta_0^2$, $D_0 = \Gamma/2\pi\delta_0^2$. The inner functions are given by

$$C_v(t) = -\log\delta + \frac{1}{2}(1+\gamma-\log 2) + \frac{4\pi^2}{\Gamma^2}\sum_{(n,m)\in\mathbb{N}^2\setminus(0,0)}^{\infty} \frac{\delta_0^4 D_n D_m A_{nm}}{n+m} 1_{\bar\nu}^{-(n+m)},$$

$$C_w(t) = -\frac{2}{\delta^2}\left[\frac{S_0}{S(t)}\right]^4 \left[\frac{m_0^2}{\Gamma^2} + \frac{8\pi^2}{\Gamma^2}\sum_{(n,m)\in\mathbb{N}^2\setminus(0,0)}^{\infty} \delta_0^4 C_n C_m A_{nm} 1_{\bar\nu}^{-(n+m)}\right],$$

where

$$A_{nm} = \int_0^\infty \mathrm{e}^{-2x} L_n(x) L_m(x)\mathrm{d}x$$
$$= \frac{(n+m)!}{n!\ m!\ 2^{m+n+1}}.$$

Let us give two examples of non-similar cores with the same circulation as the similar vortex $\zeta_0(\eta) = \Gamma\exp(-\eta^2)/\pi\delta_0^2$ of thickness δ_0. The first one is the Rankine vortex:

$$\zeta_0(\eta) = \begin{cases} \dfrac{\Gamma}{\pi\delta_0^2} & \text{if } \eta < 1, \\ \\ 0 & \text{if } \eta > 1. \end{cases}$$

The second one is the *witch-hat* vortex:

$$\zeta_0(\eta) = \begin{cases} \dfrac{\Gamma}{\pi\delta_0^2}\left(1 - \dfrac{\eta}{\sqrt{3}}\right) & \text{if } \eta < \sqrt{3}, \\ \\ 0 & \text{if } \eta > \sqrt{3}. \end{cases}$$

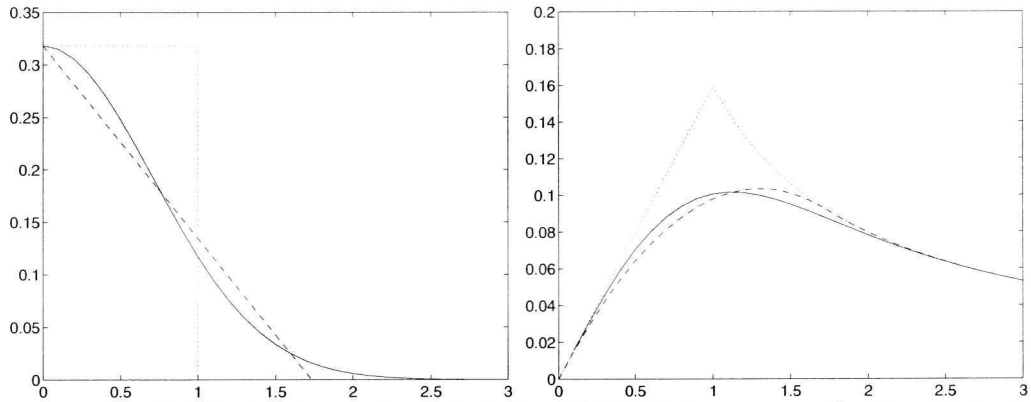

FIG. 19. Vorticity $\zeta_0\bar\delta_0^2/\Gamma$ (left) and circumferential velocity $v_0\bar\delta_0/\Gamma$ (right) versus $\eta = \bar r/\bar\delta_0$. The solid line is from the similar vortex, the dotted line for the Rankine vortex and the dashed line for the witch-hat vortex.

3. The Local Induction Approximation (LIA) equation

The Local Induction Approximation (LIA) equation is

$$\partial\mathbf{X}/\partial t = \frac{\Gamma K(s,t)}{4\pi}\left[-\log\varepsilon + \log(S) - 1 + C_v(t) + C_w(t)\right]\mathbf{b}(s,t). \tag{B2}$$

In this approximation the non-local self-induction $\mathbf{A}(s,t)$ of equation (B1) is not taken into account. This regular term is indeed negligible in the small ε limit.

4. A simple de-singularized method

One of the simplest justified de-singularized equation is [44]

$$\partial \mathbf{X}/\partial t = \frac{\Gamma}{4\pi} \int_{-\pi}^{\pi} \sigma(s',t) \frac{\mathbf{t}(s',t) \times [\mathbf{X}(s,t) - \mathbf{X}(s',t)]}{\left[|\mathbf{X}(s,t) - \mathbf{X}(s',t)|^2 + s_c^2\right]^{3/2}} \mathrm{d}s', \tag{B3}$$

with

$$s_c(s,t) = \varepsilon \exp\left[-C_v(t) - C_w(t)\right]. \tag{B4}$$

This method is very easy to implement. However, as already explained in the introduction, this equation is still stiff to be solved numerically and so needs extra discretized elements near the point on the curve where the velocity is to be computed.

5. The M1 de-singularized method of Knio and Klein

The M1 de-singularized equation of Knio and Klein [11,12] is

$$\partial \mathbf{X}/\partial t = \mathbf{v}_{\sigma_1} + (\mathbf{v}_{\sigma_1} - \mathbf{v}_{\sigma_2}) \frac{\log(\sigma_1/\delta^{ttm})}{\log(\sigma_2/\sigma_1)} \tag{B5}$$

where

$$\mathbf{v}_{\sigma_i} = \frac{\Gamma}{4\pi} \int_{-\pi}^{\pi} \sigma(s',t) \frac{\mathbf{t}(s',t) \times [\mathbf{X}(s,t) - \mathbf{X}(s',t)]}{|\mathbf{X}(s,t) - \mathbf{X}(s',t)|^3} \kappa\left(\frac{|\mathbf{X}(s,t) - \mathbf{X}(s',t)|}{\sigma_i}\right) \mathrm{d}s', i = 1,2 \tag{B6}$$

with $\kappa(r) = \tanh(r^3)$ and

$$\delta^{ttm} = \varepsilon \exp\left(C^{ttm} + 1 - C_v(t) - C_w(t)\right), \tag{B7}$$

$$\sigma_1 = 3\sigma_{max}, \tag{B8}$$

$$\sigma_2 = 2\sigma_1, \tag{B9}$$

$$\sigma_{max} = \mathrm{d}s \max_{s\in[0,2\pi]} \sigma(s,t). \tag{B10}$$

With the choice of $\kappa(r) = \tanh(r^3)$, the C^{ttm} constant is $C^{ttm} = -0.4202$ as obtained by Knio and Klein [12]. It can be computed from Eqs. (4.23), (4.22) and (3.23) of Klein and Knio [11] with a change of sign of $\zeta_{11}^{(1),ttm}$ in their equation (4.23).

Through a direct matched asymptotic expansion in σ_i of (B6) and a comparison of the associated expanded equation of motion with the Callegari and Ting (B1) equation of motion we obtain the following expression of the C^{ttm} constant

$$C^{ttm} = -\log(4) + \int_0^2 \kappa(s)/s ds + \int_2^\infty \frac{\kappa(s) - 1}{s} ds$$

for any function $\kappa(s)$ such that $\kappa(s) = 1$ at infinity. The choice of $\kappa(r) = 4\pi \int_0^r \xi^2 f(\xi) d\xi$ with $f(r) = \pi^{-3/2} \exp(-r^2)$ can be analytically computed and gives $C^{ttm} = -1 + 0.5\gamma$ where γ is the Euler's constant.

6. Mutual induction and open filaments

In case of several filaments $\mathbf{X}_j$ their induced velocities

$$\frac{\Gamma_j}{4\pi} \int_{\mathcal{C}_j} \sigma_j(s',t) \frac{\mathbf{t}_j(s',t) \times (\mathbf{X}(s,t) - \mathbf{X}_j(s',t))}{|\mathbf{X}(s,t) - \mathbf{X}_j(s',t)|^3} \mathrm{d}s', \tag{B11}$$

are added to the self-induced velocity of $\mathbf{X}$.

A periodic open filament of wavelength $\Lambda(t)$ in the axial $\mathbf{e}_x$ direction satisfies $\mathbf{X}(s+2\pi,t) = \mathbf{X}(s,t)+\Lambda(t)\mathbf{e}_x$. From Callegari and Ting's equation [10] one can deduce the following equation for such a filament:

$$\partial\mathbf{X}/\partial t = \Gamma K(s,t)\left[-\ln\varepsilon + \ln\Lambda(t) - 1 + C_v(t) + C_w(t)\right]\mathbf{b}(s,t)/4\pi + \mathbf{A}(s,t), \tag{B12}$$

where $\mathbf{A}(s,t)$ is the non-local self-induction of the filament and is given by

$$\mathbf{A}(s,t) \equiv \frac{\Gamma}{4\pi}\int_{-\infty}^{+\infty} \sigma(s+s',t)\left[\frac{\mathbf{t}(s+s',t)\times[\mathbf{X}(s,t)-\mathbf{X}(s+s',t)]}{|\mathbf{X}(s,t)-\mathbf{X}(s+s',t)|^3} - H\left(\frac{\Lambda(t)}{2} - |\lambda(s,s',t)|\right)\frac{K(s,t)\mathbf{b}(s,t)}{2\,|\lambda(s,s',t)|}\right] ds',$$

where H is the Heaviside function. The expression of the core-structure functions can be obtained by replacing the finite length $S(t)$ by the wavelength $\Lambda(t)$ of the periodic filament in the previous expressions of a closed vortex. For such a filament equations (B2), (B3) and (B5) can be rewritten in a similar way as equation (B1) becomes (B12).

APPENDIX C: EZ-VORTEX DOCUMENTATION

1. General

The EZ-Vortex package uses OpenGL for 3D rendering and has been optimized for use on SGI workstations. By using the Mesa library (public domain implementation of most OpenGL routines) it should be possible to run on virtually any machine supporting X. EZ-Vortex could be run on a PC with the Linux operating system. See http://mesa3d.sourceforge.net/ Note, you can run without graphics, but you must have OpenGL (or Mesa) header files and libraries to use the code.

This code is adapted from EZ-Scroll a Code for Simulating Scroll Waves developed by Dwight Barkley (http://www.maths.warwick.ac.uk/~barkley/ez_software.html) with courtesy of Dwight Barkley. The EZ-Vortex package (in particular this document) is under development. There are aspects of the code which ones may not be happy with, but to my knowledge everything works correctly.

The philosophy of the original code and this one is to keep programs as simple as possible and to provide documentation by way of comments within the code itself. The user is expected to modify the programs according to his or her needs. The bulk of the package is devoted to graphics. Almost all of the execution time is spent in a loop in the routine Step() in *ezstep3d.c*.

The computational methods are described in more detail in the following references. Ref. [29] describes the 3D implementation of the initial Code EZ-Scroll. Ref. [10] describes the asymptotic derivation of the Callegari and Ting equation of motion. Ref. [50,12] describes the equations and the computational methods. Ref. [11,21] describes the expansions of the Biot and Savart law. In Ref. [22] the non-similar core equation are summarized. If you generate publications from using EZ-Vortex, I ask that you cite the Margerit *et al.* paper [17].

2. Running EZ-Vortex

Files: You should have the following files:
ezvortex.c, ezstep3d.c, ezgraph3d.c, ezopengl.c, ezvortex.h, ezstep3d.h, ezgraph3d.h, ezopengl.h, task.dat, ic.m, fc.m, history.m, and *Makefile*.
You will probably want to save copies of these files (in compressed tar format).
make: It is up to you to edit *Makefile* as necessary for your system. You can either compile using SGI C (cc) or else using GNU C (gcc). You may, if you wish, specify NP (the number of point on a filament) etc. at compile time. Then these will be ignored in the task file.

Note: On an SGI, using the SGI C compiler cc with -DNP etc gives the fastest execution. Using the GNU C compiler gcc with -DNP is slightly slower and gcc without -DNP is slightly slower still. Using cc without -DNP is terrible and should not be used, i.e. if you want to specify the number of grid points through the *task.dat* file, then you should to use GNU compiler and not the SGI C compiler. This is still being looked into.

Note: in our laboratory the LOADLIBES macro in the makefile is

- SGI machine (Berlioz):
  LOADLIBES = -lGL -lX11 -lXext -lm -I/usr/include
- linux machine (Liszt):
  LOADLIBES = -I/usr/X11R6/include -L/usr/X11R6/lib/ -lGL
  -L/usr/X11R6/lib/ -lX11 -lm

Make *ezvortex* by typing *make*. Then run by typing *ezvortex*. A window should open containing an initial condition for the vorticity field, i.e. one or several closed or open filaments. The centerlines of the filaments are plotted. Hitting the space bar in the EZ-Vortex window will start the simulation. This is a coarse resolution run showing the speed possible with EZ-Vortex simulations. With the pointer in the EZ-Vortex window, you can:

(1) Switch between curve display, worm display and no field by typing *c*, *w*, or *n* respectively. The worm display is a tube display with a thickness that allows to have a 3D view without rotating. Without rotating, no 3D view can be seen from the curve display. The tube radius is only geometrical: it is not linked to the physical radius which may change due to the global stretching or to diffusion.

(2) Pause the simulation by typing *p*, and resume by typing a *space*.

(3) Rotate the image by first pausing the simulation, then by holding down the left mouse button and moving the cursor.

(4) The key r resets the view to the initial (start up) view, and z sets the view to looking down the z-axis with the x- and y-axes in the usual orientation. This view is useful for moving the image.

(5) The arrow keys move the image in the x-y directions. The + key moves the image up the z-axis and the − moves it down the z-axis. Again, for moving the image it is best first to have set the view by typing z.

(6) Stop the simulation by typing:
q for soft termination with all files closed or
ESC for immediate termination without writing final conditions (equivalent to typing control-C from the shell).

(7) Snapshot the window (on a SGI workstation) by typing s

After a successful run, you will have a file *fc.dat* in your directory which contains the final conditions of the run. If you copy this file to *ic.dat*, then the next time you run *ezvortex*, this file will be read and used as an initial condition. (The files *ic_dat.m* and *fc_dat.m* are Matlab files that can also be used to see initial and final conditions.)

3. Equations

You have the choice between four equations of vortex filament motion which are implemented in *ezvortex.h*. These equations are given in Appendix B.

4. Compilation Macros

The main compilation parameters are in *ezvortex.h*:

- You can choose the equation of motion whether the macros LOCAL_INDUCTION, CALL_AND_TING, DE_SINGU, and M1_KNIO_KLEIN are set to 1 or 0.
- You can choose closed or open filament whether the macro CLOSED is set to 1 or 0.
- You can have graphics or not at run time whether the macro GRAPHICS is set to 1 or 0.
- You can snapshot different history steps if the macro MOVIE is set to 1 (only on a SGI work station).
- You can run a *history.dat* file instead of computing whether the macro COMPUTE is set to 1 or 0.
- You can have a non-similar part of the core or not whether the macro NON_SIMIL_PART is set to 1 or 0. The macro SIMIL_PART has to be set to 1 in any case.
- You can have an uniform core by setting the macro SIMIL_PART to 0 and the macro UNIFORM_CORE to 1 (to be coherent you have to choose nu_bar=0 in *task.dat*).
- You can choose to have spectral spatial derivative or not by setting the macro SPECTRAL to 1 or 0.
- You can choose to have an explicit (order 1) time stepping with the macro EXPLICIT, an implicit one with the macro NEWTON, and an explicit Adams-Bashforth with the macro ADAMS_BASHFORTH. The explicit methods (order 1 or Adams Bashforth) can be performed either with a Jacobi iteration or a Gauss-Seidel one whether the macro GAUSS_SEIDEL is set to 0 or 1. The Callegari and Ting method and the LIA method are numerically instable with an explicit (order 1 or Adams Bashforth) scheme either a Jacobi or a Gauss-Seidel stepping is used. The M1 Knio and Klein method is stable with an explicit scheme.
- You can test the convergence of the Biot-Savart velocity computation at initial time if the macro CONV_ANALYSE is set to 1. A file *look* is then generated with three columns associated to the three components of the velocity on the filament. The convergence can be assess with the number of point and also with the number of periodic boxes for open filaments.
- You can have an automatic motion of the graphic window in the z direction or not whether the macro MOVE is set to 1 or 0.

5. Parameters

The parameters are either set in the routine Generate_ic() at the end of *ezvortex.c* when these vortices are initially created or in the file *task.dat*. The parameters of *task.dat* are loaded at the beginning of a run and so you need not to re-compile *ezvortex* when these parameters are changed.

In the case of similar vortex filaments delta_0_bar_param is the initial stretched core radius δ_0, m_0_param is the initial axial flux m_0, gamma_param is the circulation Γ, and epsilon is the reduced thickness ε. They are parameters of the core structure. nu_bar is the stretched viscosity ν of the fluid. Thus the "physical" parameters in the simulation are: delta_0_bar_param, m_0_param, gamma_param, epsilon, nu_bar and nf the number of filaments. The parameters delta_0_bar_param, m_0_param, gamma_param are selected for each filaments in the routine Generate_ic() at the end of *ezvortex.c* when these vortices are initially created. The parameters epsilon and nu_bar are set in the file *task.dat*.

The "numerical" parameters for the simulation are: np = number of spatial points in each filament, ts = time step, n_b = number of periodic boxes (for open filaments) and are also set in the file *task.dat*.

The other parameters set in *task.dat* are:

Number of time steps to take

Time steps per plot. Also set the number of time steps per filament computation.

error_stop. Error to stop the Newton iteration for the implicit method.

Time steps per write to history file and of snapshot if MOVIE is set to 1 in *ezvortex.h*

initial field display : curve or worm

initial condition type : from 0 to 12.

output type : ascii or binary

verbose

These are more or less self-explanatory.

If Time steps per write is non-zero then the filament data will be written to a file (*history.dat*) every Time steps per write (whether or not there is any graphics) which can be executed by *ezvortex* with the macro COMPUTE set to 1. (The filaments will also be saved every Time steps per write to a file (*history_dat.m*) which can be executed with matlab.)

I leave it to you to look at different initial condition types at the end of *task.dat* and *ezvortex.c*. The number of filaments nf set has to be coherent with the initial condition chosen. You can choose between :

(0) Oscillations of a Vortex Ring (Standing wave)
(1) Oscillations of an ellipse in a plan y-z
(2) Oscillations of a Vortex Ring (Travelling wave)
(3) Oscillations of a triangle Vortex Ring
(4) Motion of a Lissajous ring
(5) Motion of two side by side vortex rings
(6) Leap frogging of two vortex rings
(7) Motion of two face to face (and shifted) vortex rings
(8) Motion of two face to face vortex rings
(9) Motion of two linked vortex rings
(10) Motion of two vortex rings
(11) Oscillations of a straight filament
(12) Motion of a helical filament
(13) Oscillation of two trailing vortices
(14) Crow instability of two trailing vortices
(15) Crow instability of two trailing vortices (initially at most instable angle)

The other place to look for "parameters" is in the header files. The main compilation parameters are in *ezvortex.h*. Many of the macro definitions in the other header files can be replaced with variables.

APPENDIX D: VALIDATION AGAINST EXACT SOLUTIONS AND LINEAR STABILITY RESULTS

In this appendix we validate the code EZ-vortex against known solutions of the equations of motion for the centerline and results of linear stability studies. We also give the values of the numerical parameters that give converged numerical results for the different configurations under consideration. All following simulations use the M1 de-singularized method of Knio and Klein with the explicit Adams-Bashforth scheme, there is no axial flow ($m_0 = 0$) and the fluid is inviscid ($\nu = 0$). Here, the vortex core is similar and $\Gamma = 1$. As the initial reduced thickness is $\delta_0 = 1$ the small parameter ε is the initial thickness δ_0.

1. The perturbed circular vortex ring

The velocity of a circular vortex ring of radius R and thickness δ is [50,51]

$$V = \frac{\Gamma}{4\pi R}\left(\log\frac{8R}{\delta} + C_v - 1 + C_w\right). \tag{D1}$$

For a similar core without axial velocity $C_v = 0.442$ and $C_w = 0$. In figure 20 we plot the velocity V of the vortex ring of radius $R = 1$ as a function of the initial thickness ε. Numerical results (crosses) are in excellent agreement with the analytical result (solid line). The numerical parameters of the computation are given in Table IX for the M1 method of Knio and Klein with the explicit Adams-Bashforth scheme (Run 1) or for the Callegari and Ting equation with an implicit iteration (Run 2).

The period T of a modal perturbation with azimuthal wavenumber n is

$$T = \frac{8\pi^2 R^2}{\Gamma\sqrt{[n^2\tilde{V}_0 - g_\xi(n)][(n^2-1)\tilde{V}_0 + g_\rho(n)]}}, \tag{D2}$$

where $\tilde{V}_0 = 4\pi RV/\Gamma$ and $[g_\xi(n), g_\rho(n)]$ are given in Margerit *et al.* [50]. In figure 21 we plot the period T for the mode 3 of the perturbed vortex ring as a function of ε. Numerical results (crosses in Fig. 21 and Run 3 in Table IX) are in excellent agreement with the analytical result (solid line). The initial amplitude of the perturbation is $\rho_0 = 0.01$ with the centerline in a plane. This period is found by using $\rho_\perp$ the amplitude part orthogonal to the propagating direction x. It is given by $\rho_\perp = \mathrm{abs}[\sqrt{Z^2+Y^2} - \mathrm{mean}(\sqrt{Z^2+Y^2})]$ where $\mathbf{X} = (X, Y, Z)$ and where *mean* is the spatial average on the filament at time t. The pulsation is then found with the slope of the temporal function $\arccos[\rho_\perp/\rho_\perp(0)]$. This slope does not depend on the point of abscisse s that is used. In practice we do not choose any point and use the maximum of $\rho_\perp$ over the filament. It converges with all numerical parameters (time step, number of points) and with decreasing initial amplitude ρ_0.

TABLE IX. Numerical parameters: closed vortices

	Run	np	dt	nsteps	CPU time*(s)
Vortex Ring Velocity:M1	1	101	0.0016	7000	79.8
// :CT	2	//	//	//	186
Vortex Ring Period	3	257	0.0016	250	17
Vortex Ring Pair	4	101	0.00008125	7000	1200

*SGI R10000 work-station at 225MHz

The period at $\varepsilon = 0.15$ is not exactly on the curve. This small difference comes from finite ε effect. M1 Knio and Klein method and Callegari and Ting equation has been proved to be equivalent in the asymptotic small ε limit. When $\varepsilon = 0.15$ we notice (figure 22) a difference of the Biot-Savart results given by these two methods whereas there is no difference for $\varepsilon = 0.02$. We believe that this difference is due to the next-order correction in ε which may no longer be neglected at $\varepsilon = 0.15$. All methods and stability equations are equivalent at leading order but may be slightly different due to the effect of next-order correction.

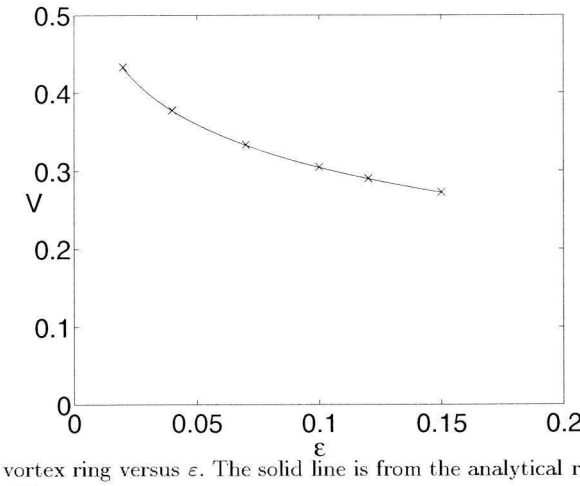

FIG. 20. Velocity V of the vortex ring versus ε. The solid line is from the analytical result and crosses from numerical computation (Run 1 in Table IX).

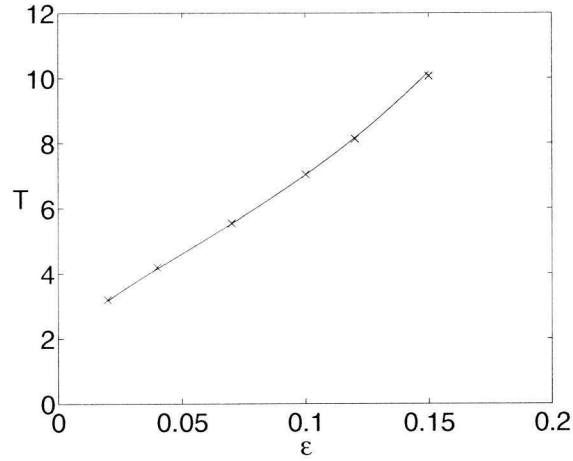

FIG. 21. Period T for the mode 3 of the perturbed vortex ring versus ε. Same legend as in Fig. 20

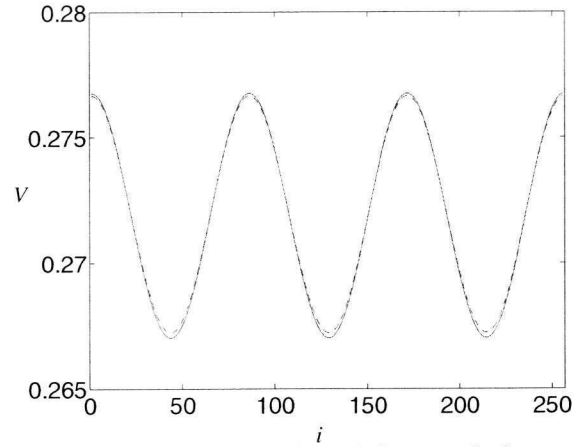

FIG. 22. Binormal velocity V at initial time for the mode 3 of the perturbed vortex ring $\varepsilon = 0.15$ versus the node number i of the filament. The solid line is the M1 Knio and Klein method and the dashed line is the Callegari and Ting equation. Same parameters as in Fig. 21.

2. Motion of a vortex ring pair

We consider two circular vortex rings in the same plane with same center and thickness δ. Let Γ_o, Γ_i, R_o and R_i denote the circulations and the radius of the outer and inner vortices. We introduce the dimensionless parameters $R = R_i/R_o$ and $G = \Gamma_i/\Gamma_o$. There is an exact stationary solution of the equation of motion (B1) provided that the following relation between G and R is satisfied [52]

$$G = \frac{E(k)/(1-R) + K(k)/(1+R) - 0.5\,[\log(8R_0/\delta) + C_v - 1 + C_w]}{-E(k)/(1-R) + K(k)/(1+R) - 0.5\,[\log(8R_i/\delta) + C_v - 1 + C_w]/R}, \tag{D3}$$

where $k = 2\sqrt{R}/(1+R)$. Here E and K are complete elliptic integrals of second and first kinds. The associated velocity V is

$$V = \frac{\Gamma_i}{4\pi R_i}\,[\log(8R_i/\delta) + C_v - 1 + C_w] + \frac{\Gamma_o}{2\pi R_o}\,[E(k)/(1-R) + K(k)/(1+R)]\,. \tag{D4}$$

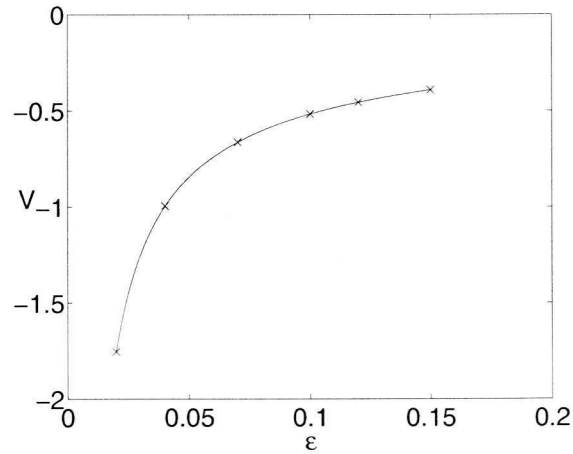

FIG. 23. Velocity V of the vortex ring pair versus ε for $R = 0.5$ Same legend as in Fig. 20

In figure 23 we plot the velocity V of the vortex ring pair as a function of ε for $R = 0.5$ and $\Gamma_i = 1$. Numerical results (crosses in Fig. 23 and Run 4 in Table IX) are in excellent agreement with the analytical result (solid line).

3. The perturbed straight filament

The period of rotation of a sinusoidal perturbation on a straight filament is

$$T = \frac{8\pi^2}{\Gamma k^2 |1/2 - \gamma + \log(2/\delta k) + C_v - 1 + C_w|}, \tag{D5}$$

where $\gamma = 0.577215$, δ is the core radius, Γ is the circulation and $k = 2\pi/\Lambda$ is the wave number. This result generalizes to an arbitrary vorticity profile the classical Kelvin [53] result for the bending modes of a Rankine vortex for small wave-numbers. Kelvin obtained it by considering infinitesimal perturbations to a columnar vortex; we obtained it by infinitesimal perturbations to the straight centerline in (B12).

In figure 24 we plot the period T for the wavelength $\Lambda = 1.25$ of the perturbed straight vortex filament as a function of ε. Numerical results (crosses in Fig. 24 and Run 5 in Table I) are in excellent agreement with the analytical result (solid line). The initial amplitude of the perturbation is $\rho_0 = 0.01$. This period is found by using ρ_y the amplitude part in the y direction. It is given by $\rho_y = \mathrm{abs}(Y - Y)$ where $\mathbf{X} = (X, Y, Z)$ and where Y is the spatial average on the filament at time t. The pulsation is then found with the slope of the temporal function $\arccos[\rho_y/\rho_y(0)]$.

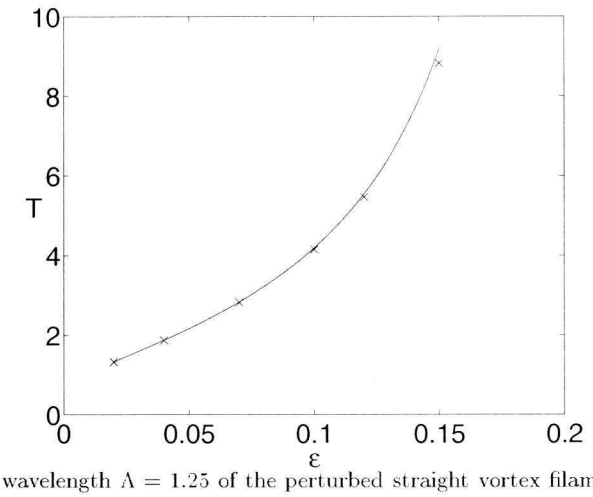

FIG. 24. Period T for the wavelength $\Lambda = 1.25$ of the perturbed straight vortex filament versus the initial thickness ε. Same legend as in Fig. 20.

[1] K. Huenecke, Vortex wakes from large aircraft - A challenge for industrial research. *AIAA Paper* 2000-2216(2000).
[2] T. Gerz, F. Holzaepfel, and D. Darracq, Aircraft Wake Vortices. A Position Paper. In: *5th WakeNet Workshop on Wake Turbulence and the Airport Environment.* Langen, Germany(2001).
[3] P. R. Spalart, Airplane Trailling Vortices. *Annual Review of Fluid Mechanics* 30(1998) 107–138.
[4] D. Knözer(1999), C-wake Project (Wake vortex characterization and control):. Technical Report GRD1-1999-10332, EU. p.76-77.
[5] E. G. Puckett, Vortex Methods: An Introduction and Survey of Selected Research Topics. In: R. A. Nicolaides and M. D. Gunzburger (eds.): *Incompressible Computational Fluid Dynamics - Trends and Advances.* pp. 335–407(1993).
[6] G.-H. Cottet and P. Koumoutsakos, *Vortex methods: theory and practice.* Cambridge: Cambridge University Press(2000).
[7] J. Marshall, P. Brancher, and A. Giovannini, Interaction of inequal anti-parallel vortex tubes. *J. Fluid Mech.* 446(2001) 229–252.
[8] A. Giovannini, Validation of a three dimensional partical method. (2002). to be submitted.
[9] D. Margerit, P. Brancher, and A. Giovannini, Implementation and validation of a slender vortex filament code: Its application to the study of a four-vortex wake model. *submitted to Int. J. Numer. Meth. Fluids.*
[10] A. Callegari and L. Ting, Motion of a curved vortex filament with decaying vortical core and axial velocity. *SIAM J. Appl. Math.* 35(1)(1978) 148–175.
[11] R. Klein and O. Knio, Asymptotic vorticity structure and numerical simulation of slender vortex filaments. *J. Fluid Mech.* 284(1995) 257–321.
[12] O. Knio and R. Klein, Improved thin-tube models for slender vortex simulations. *J. Comput. Phys.* 163(1)(2000) 68–82.
[13] T. Ehret and H. Oertel, Calculation of wake vortex structures in the near-field wake behind cruising aircraft. *Atmospheric Environment* 32(18)(1998) 3089–3095.
[14] A. C. Bruin(2001), Test report for wake survey tests behind SWIM model geometry in DNW-LST and DNW-LLF wind tunnels. Technical Report TR-2001-183, NLR.
[15] M. E. Hamraoui, Contributions à la simulation d'écoulement tridimensionnel par méthode de vortex. Ph.D. thesis, University of Toulouse III(1999).
[16] J. R. Mansfield, O. Knio, and C. Meneveau, Dynamic LES of colliding vortex rings using a 3D vortex method. *J Comput Phys* 152(1999) 305–345.
[17] D. Margerit, A. Giovannini, and P. Brancher(2001), EZ-Vortex documentation: a Slender Vortex Filament solver. IMFT report.
[18] D. Fabre and L. Jacquin, Stability of a four-vortex aircraft wake model. *Phys. Fluids* 12(10)(2000) 2438–2443.
[19] D.Fabre, Instabilités et instationnarités dans les tourbillons : Application aux sillages d'avions. Ph.D. thesis, Paris VI(2002).
[20] S. C. Rennich and S. K. Lele, A method for accelerating the destruction of aircraft wake vortices. *AIAA Paper* 98-0667(1998) 1–11.
[21] D. Margerit and J.-P. Brancher, Asymptotic Expansions of the Biot-Savart law for a slender vortex with core variation. *Journal of Engineering Mathematics* 40(3)(2001) 297–313.
[22] D. Margerit, Axial core-variation of axisymmetric shape on a curved slender vortex filament with a Batchelor, Rankine, or bubble core. in revision for Phys. Fluids.
[23] M. Rossi, Of vortices and vortical layers: An overview. In: A. Maurel and P. Petitjeans (eds.): *Lectures of a Workshop Held in Rouen.* Berlin Heidelberg, pp. 40–123(2000).
[24] A. C. Bruin(2001), Set with 6 CD-Roms with data of the C-Wake test campaign with the SWIM model in LST.
[25] A. C. Bruin and F. Ganzevles(2001), Set with 1 CD-Rom with reprocessed data of the C-Wake test campaign with the SWIM model in LST and LLF.
[26] A. C. Bruin and F. Ganzevles(2001), Data analysis of wake survey tests behind SWIM model in DNW-LST and DNW-LLF wind tunnels. Technical Report TR-2001-201, NLR.
[27] A. C. Bruin and F. Ganzevles(2002), A correction procedure for two-component PIV measurments. Technical Report TR-2002-, NLR.
[28] D. Barkley, A model for fast computer simulation of waves in excitable media. *Physica D* 49(1991) 61–70.
[29] M. Dowle, R. M. Mantel, and D. Barkley, Fast simulations of waves in three-dimensional excitable media. *Int. J. of Bifurcation and Chaos* 7(11)(1997) 2529–2545.
[30] C. Liu, J. Tavantzis, and L. Ting, Numerical Studies of Motion of Vortex Filaments-Implementing the Asymptotic Analysis. *AIAA Paper* 84-1542(1984) 1–11.
[31] S. Crow, Stability theory for a pair of trailing vortices. *AIAA J.* 8(1970) 2172–2179.
[32] L. Ting and R. Klein, *Viscous Vortical Flows (Monograph).* Lecture Notes in Physics(1991).
[33] L. Ting and F. Bauer, Viscous Vortices in two- and three-Dimensional Space. *Computer Fluids* 22(N 4/5)(1993)

565–588.
[34] A. Leonard, Numerical simulation of interacting, three-dimensional vortex filaments. In: *4th International Conference on Numerical Methods in Fluid Dynamics*. New York, pp. 245–250(1975).
[35] A. Corjon and T. Poinsot, Vortex model to define safe aircraft separations distances. *J. Aircraft* 33(3)(1996) 547–554.
[36] J.-C. J. Saghbini and A. F. Ghoniem, Numerical simulation of the dynamics and mixing in a swirling flow. *AIAA Paper* 97-0507(1997).
[37] J. D. Crouch, Instability and transient growth for two trailling-vortex pairs. *J. Fluid Mech.* 350(1997) 311–330.
[38] D. Margerit, The complete first order expansion of a slender vortex ring. In: E. Krause and K. Gersten (eds.): *IUTAM Symposium on Dynamics of Slender Vortices*. Aachen, pp. 45–54(31 Aug.-3 Sep. 1997).
[39] F. Laporte and A. Corjon, Direct Numerical Simulation of elliptic instability of a vortex pair. *Phys. Fluids* 12(5)(2000) 1016–1031.
[40] G. Batchelor, *Introduction to fluid dynamics*. Cambridge: Cambridge University Press(1967).
[41] P. Saffman, *Vortex dynamics*. Cambridge: Cambridge University Press. 33-38, 208-215(1992).
[42] L. Ting, Studies in the motion and decay of vortices. In: J. Olsen, A. Goldburg, and R. Rogers (eds.): *Proc. Symposium on Aircraft Wake Turbulence*. Seattle, Washington, pp. 11–39(1971).
[43] C. Liu, J. Tavantzis, and L. Ting, Numerical studies of motion and decay of vortex filaments. *AIAA Journal* 24(8)(1986) 1290–1297.
[44] A. Leonard, Computing three-dimensional incompressible flows with vortex elements. *Ann. Rev. Fluid Mech.* 17(1985) 523–559.
[45] F. Hama, Progressive deformation of a curved vortex filament by its own induction. *Phys. Fluids* 5(1962) 1156–1162.
[46] S. Widnall and J. Sullivan, On the stability of vortex rings. *Proc. R. Soc. London A* 332(1973) 335–353.
[47] S. Widnall, D. Bliss, and A. Zalay, Theoretical and experimental study of the stability of a vortex pair. In: J. Olsen, A. Goldburg, and R. Rogers (eds.): *Proc. Symposium on Aircraft Wake Turbulence*. Seattle, Washington, pp. 305–338(1971).
[48] S. Widnall, The structure and dynamics of vortex filaments. *Annual Review of Fluid Mechanics* 7(1975) 141–165.
[49] D. Moore and P. Saffman, The motion of a vortex filament with axial flow. *Philos. Trans. Roy. Soc. London Ser. A* 1226(272)(1972) 403–429.
[50] D. Margerit and J.-P. Brancher, Motion and oscillations of a circular perturbed vortex ring. *C. R. Acad. Sci. Paris, Série II b* 328(2000) 1–6.
[51] D. Margerit, Mouvement et dynamique des filaments et des anneaux tourbillons de faible épaisseur. Ph.D. thesis, Institut National Polytechnique de Lorraine(1997).
[52] P. D. Wedman and N. Riley, Vortex ring pairs: numerical simulation and experiment. *J. Fluid Mech.* 257(1993) 311–337.
[53] Kelvin, Vibration of a columnar vortex. *Philos. Mag.* 10(1880) 152–165.